Department of Chemistry

University of Helsinki

Faculty of Science

New noble-gas compounds and environmental effects

Cheng Zhu

ACADEMIC DISSERTATION

To be presented, with the permission of the Faculty of Science of the University of Helsinki, for public examination in lecture hall A110 of the Department of Chemistry (A. I. Virtasen aukio 1) on March 29th, 2016, at 12 o'clock.

Helsinki 2016

Supervisors

Docent Leonid Khriachtchev
Professor Markku Räsänen
Department of Chemistry
University of Helsinki

Reviewers
Professor Vladimir I. Feldman
Department of Chemistry
Lomonosov Moscow State University
and
Professor Li Sheng
Department of Chemistry
Harbin Institute of Technology

Opponent
Professor Pettersson Mika
Department of Chemistry
University of Jyväskylä

ISBN 978-951-51-2013-7 (paperback)
ISBN 978-951-51-2014-4 (PDF)
Unigrafia
Helsinki 2016

Abstract

Noble-gas chemistry was started in 1962 when Neil Bartlett reported the first noble-gas compound, xenon hexafluoroplatinate. This discovery was followed by successful synthesis of many other noble-gas compounds. Matrix-isolation infrared spectroscopy has been an important tool in noble-gas chemistry. In 1995, noble-gas hydrides HNgY (Ng is a noble-gas atom and Y is an electronegative fragment) were characterized by using this method. To date, a substantial number of noble-gas hydrides have been identified including the first neutral ground-state Ar compound, HArF. A few noble-gas compounds of the YNgY' type (Y and Y' are electronegative fragments) have also been prepared in matrices.

This thesis consists of two parts. In the first part, two new HNgY compounds (HKrCCCl and HXeCCCl) and three new YNgY' compounds (FKrCN, FXeCN, and FXeNC) are described. These molecules are prepared in noble-gas matrices (Kr and Xe) by ultraviolet photolysis of the precursors and subsequent annealing and characterized by infrared spectroscopy. The assignments are supported by *ab initio* calculations at the MP2(full) and CCSD(T) levels of theory. The precursors HCCCl and FCN are synthesized using a microwave discharge of $HClC{=}CCl_2$/Ng and $(FCN)_3$/Ng gaseous mixtures, respectively. The infrared spectrum of CCCl radical is also reported.

In the second part, the complexation effect on HXeI and the matrix effect on HXeI and HXeH are studied. Two new complexes (HXeI···HCl and HXeI···HCCH) are prepared in a Xe matrix and assigned based on the *ab initio* calculations at the MP2(full) and CCSD(T) levels of theory. Similarly to the previously studied systems, the H–Xe stretching mode of HXeI in these complexes show substantial blue shifts. The decomposition of the HXeI complexes (including known HXeI···HBr and HXeI···HI) by broadband IR radiation of the spectrometer slows down as the H–Xe stretching frequency increases.

HXeI and HXeH are studied in Ar, Kr, and Xe matrices. The order of the H–Xe stretching frequency of HXeH in these matrices (ν(Xe) < ν(Kr) < ν(Ar)) is the same as that of previously studied HXeCl, HXeBr, and HXeCCH. For HXeI, the frequency order is different: ν(Xe) < ν(Ar) < ν(Kr), which is a remarkable observation. The experimental results are successfully simulated using the hybrid quantum-classical calculations.

Acknowledgements

I would like to express my sincere gratitude to all those who have supported me over the last three and half years for completing my PhD study. First of all, I am grateful to Prof. Markku Räsänen for giving me the exquisite opportunity to study at the University of Helsinki and providing necessary support during this work. I am deeply indebted to Doc. Leonid Khriachtchev for sharing his vast scientific experience and providing invaluable guidance during the research. Dr. Masashi Tsuge is acknowledged for introducing me to the field of matrix isolation and sharing his experimental and computational skills. All co-authors of my papers are thanked for their fruitful contributions, suggestions, and collaborations.

I sincerely thank the pre-examiners of this thesis, Prof. Vladimir I. Feldman (Lomonosov Moscow State University) and Prof. Li Sheng (Harbin Institute of Technology), for their encouraging comments on my thesis.

I also wish to acknowledge the head of our laboratory, Prof. Lauri Halonen, and all other researchers and staff of our laboratory for creating a friendly and supportive working atmosphere. I sincerely thank Dr. Luis Duarte and Doc. Markus Metsälä for their great assistance. I also appreciate my colleagues (Qian Cao, Susy Lopes, Heidi Reiman, and Sergey Ryazantsev) and my Chinese friends (Juan Hong, Jianyong Li, Xia Yu, Wen Chen, and all the others) in Helsinki for their company and help. My family are deeply thanked for their love and support.

Finally, I appreciate the financial support from the China Scholarship Council, several research projects from the Academy of Finland, and the travel grant from the doctoral programme in Chemistry and Molecular Sciences.

List of publications

This thesis is based on the following publications:

I. C. Zhu, M. Räsänen, and L. Khriachtchev,
Matrix-isolation and ab initio study of HKrCCCl and HXeCCCl
J. Chem. Phys. **143**, 244316 (2015).

II. C. Zhu, M. Räsänen, and L. Khriachtchev,
Fluorinated noble-gas cyanides FKrCN, FXeCN, and FXeNC.
J. Chem. Phys. **143**, 074306 (2015).

III. C. Zhu, M. Tsuge, M. Räsänen, and L. Khriachtchev,
Experimental and theoretical study of the HXeI···HCl and HXeI···HCCH complexes.
J. Chem. Phys. **142**, 144306 (2015).

IV. C. Zhu, K. Niimi, T. Taketsugu, M. Tsuge, A. Nakayama, and L. Khriachtchev,
HXeI and HXeH in Ar, Kr, and Xe matrices: Experiment and simulation.
J. Chem. Phys. **142**, 054305 (2015).

The candidate, Cheng Zhu, has done most of the experimental work in these publications. He has performed all calculations in publications I and II. Other calculations were provided by Masashi Tsuge (publication III) and Keisuke Niimi, Tetsuya Taketsugu, and Akira Nakayama (publication IV). The candidate participated in preparation of the publications (especially I, II, and III).

Contents

Abstract 3
Acknowledgements 4
List of publications 5
Contents 6
1. Introduction 7
1.1 Brief history of noble-gas compounds 7
1.2 Environmental effects 8
1.3 Motivation 9
2. Methods 11
2.1 Experimental methods 11
2.2 Computational methods 12
3. New noble-gas compounds 14
3.1 Computational results 14
3.1.1 Structure and charge distribution 14
3.1.2 Energetics 16
3.1.3 Vibrational properties 17
3.2 Experimental results 18
3.2.1 HKrCCCl and HXeCCCl 18
3.2.2 FKrCN, FXeCN, and FXeNC 22
3.3 Discussion 24
4 Environmental effects 28
4.1 Complexes of HXeI 28
4.1.1 Computational results 28
4.1.2 Experimental results 31
4.1.3 Discussion 34
4.2 Matrix effect on HXeI and HXeH 36
4.2.1 Computational results 36
4.2.2 Experimental results 38
4.2.3 Discussion 40
5. Results in brief 42
References 44

1. Introduction

1.1 Brief history of noble-gas compounds

The former name of noble (rare) gases was inert gases, which indicated their low chemical reactivity. This name was deprecated after noble-gas compounds were found. Kossel (1916),[1] von Antropoff (1924),[2] and Pauling (1933)[3] suggested that Kr and Xe could be reactive. However, the early attempts to synthesize noble-gas compounds were unsuccessful. The breakthrough in experimental noble-gas chemistry came in 1962 when Neil Bartlett reported Xe hexafluoroplatinate $Xe^{+}[PtF_6]^{-}$.[4] Many other Xe compounds have been found later.[5-12] The first Xe–O bond in $XeOF_4$ was reported in 1963.[5] In 1967, Nelson and Pimentel synthesized the compound with the Xe–Cl bond ($XeCl_2$) in a low-temperature Xe matrix.[13] Goetschel and Loos introduced the Xe–B bond in $FXeBF_2$ in 1972.[14] In 1974, the formation of $FXeN(SO_2F)_2$ demonstrated the Xe–N bond.[15] The first Xe–C bond was found in $Xe(CF_3)_2$.[16] The latest new Xe bond is probably the Xe–Au bond in $[AuXe_4^{2+}][Sb_2F_{11}^{-}]_2$, which was reported by Seidel and Seppelt in 2000.[17]

Kr chemistry is less extensive.[10,11,18] Kr difluoride, the first Kr compound, was prepared by irradiation of a F_2/Kr/Ar solid matrix at 20 K by a medium-pressure mercury lamp and characterized by infrared spectroscopy by Turner and Pimentel in 1963.[19] The Kr–N bond in $[HCNKrF]^{+}[AsF_6]^{-}$ was discovered by Schrobilgen in 1988.[20] One year later, Sanders and Schrobilgen identified $Kr(OTeF_5)_2$, which contained the Kr–O bond.[21]

Noble-gas hydrides HNgY, where Ng is a noble-gas atom and Y is an electronegative fragment, were discovered in 1995.[22] The first molecules of this family were HXeI, HXeBr, HXeCl, HKrCl, and HXeH.[22,23] Up to now, a substantial number of noble-gas hydrides have been identified including the neutral ground-state Ar compound, HArF.[24,25] Most of the HNgY molecules have been characterized in noble-gas matrices by using infrared spectroscopy.[11,25] A few of them have also been found in gas-phase Xe clusters.[26-28] Typical synthesis of a HNgY molecule in a noble-gas matrix includes two steps: (i) UV photolysis of HY precursors to form the H + Y fragments and (ii) annealing of the matrix to mobilize the H atoms and promote the $H + Ng + Y \rightarrow HNgY$ reaction.[11,25] Irradiation by fast electrons and X-rays has also been used to prepare HNgY molecules.[29-33] A number of new chemical bonds (e.g., Xe–S, Xe–I, Kr–C, Kr–Cl, H–Ar, and Ar–F) have been found in noble-gas hydrides.

The HNgY molecules can be presented in the form $(HNg)^{+}Y^{-}$ where the $(HNg)^{+}$ bonding is mainly covalent and the interaction between $(HNg)^{+}$ and Y^{-} is predominantly ionic.[25] These molecules are high-energy metastable species with respect to the HY + Ng fragments, but the decomposition via the two-body (2B) decomposition channel $HNgY \rightarrow Ng + HY$ is prevented by high barriers.[25] All experimentally prepared HNgY molecules are lower in energy than the

three-body (3B) dissociation asymptote H + Ng + Y, which allows their formation at low temperatures.[25,34]

In the experiments with HCCF in a Kr matrix, in addition to HKrCCF, a molecule of a different type, FKrCCH, was observed.[35] The latter molecule can be represented by the formula YNgY' where Y and Y' are two different electronegative fragments. The first molecule of this type was most probably FXeCl.[36] Using the ClCN and BrCN precursors, three new molecules of this type, ClXeCN, ClXeNC, and BrXeCN, were prepared in a Xe matrix.[37] A number of similar species have been predicted by quantum chemical calculations.[38-42]

1.2 Environmental effects

Non-covalent interactions are responsible for many properties of matter and play an important role in chemical reactions.[43-46] The intermolecular interactions can be successfully studied by vibrational spectroscopy because they change the characteristic vibrational frequencies of the interacting molecules. In particular, matrix-isolation infrared spectroscopy has been extensively used to study intermolecular interactions.[47-61]

Noble-gas hydrides are characterized by weak bonding and large dipole moments, which leads to a strong complexation effect on their vibrational properties. [11,25,61-82] Nemukhin *et al.* observed the complex of HXeOH with water in a Xe matrix.[62] Corani *et al.* identified the HKrCl···HCl complex in a Kr matrix.[68] Other examples of the experimentally studied HNgY complexes include HArF···N_2,[64] HXeBr···HBr,[67] HXeBr···CO_2,[70] HXeI···HI,[71] HKrCCH···HCCH,[73] *etc*. It has been experimentally found that the H−Ng stretching modes in these complexes exhibit blue shifts with respect to the HNgY monomers. For example, the H–Kr stretching frequencies of HKrCl···HCl are shifted by up to +306 cm^{-1} from the HKrCl monomer,[68] which is probably the largest experimentally observed blue shift for 1:1 complexes. The computational results show that the $(HNg)^+Y^-$ ion-pair character of the HNgY molecules is enhanced upon complexation. As a result, the HNg entity of these molecules becomes closer to the properties of the free HNg^+ cation with a shorter bond length, higher H–Ng stretching frequency, and lower IR absorption intensity.[66]

Many computational studies on the complexes of noble-gas hydrides are known.[62,74-82] McDowell reported that the HArF···HF complex exhibits a very large blue shift of the H–Ar stretching mode and a red shift of the HF stretching mode.[75] As an important issue, the stabilization/destabilization complexation effects on noble-gas hydrides have been studied computationally. Nemukhin *et al.* found that in the HXeOH···$(H_2O)_n$ complexes, the surrounding water molecules decrease the 2B decomposition barrier of HXeOH, and it becomes unstable for $n \geq 4$.[62] On the other hand, Tsivion and Gerber reported that HXeCCH is stable in HCCH clusters even at elevated temperature (150 K).[83] For noble-gas hydride clusters, *ab initio* calculations show that $(HXeH)_n$ (n = 2, 3, and 4)[76] and $(HXeCCH)_n$ (n = 2 and 4)[79] are stable whereas $(HArF)_2$ is unstable.[77]

The matrix is known to change the properties of embedded species (solvation effect).[84-86] HXeCl, HXeBr, and HXeCCH have been studied in Ne, Ar, Kr, and Xe matrices.[22,87-91] The observation of HXeCl, HXeBr, and HXeCCH in a Ne matrix suggests their intrinsic stability. The frequency order of the H–Xe stretching mode of these molecules is found to be ν(Ar) > ν(Kr) > ν(Xe) > ν(Ne). Apparently, the matrix shift of this mode is non-monotonous with respect to the polarizability of the noble-gases atoms Ar, Kr, and Xe. Some of HNgY molecules have been prepared in molecular matrices (CO_2 and N_2).[70,90]

Several theoretical works has attempted to explain the matrix effect on the HNgY molecules. The calculations of the 1:1 HNgY···Ng complexes and the polarizable continuum model (PCM) have failed to explain the observed blue-shifts of the H–Xe stretching mode in Ar and Kr matrices compared to a Xe matrix.[89,90] The recent works using bigger HNgY@Ng′$_n$ systems and more sophisticated computational methods have provided better results. Kalinowski *et al.* performed the MP4(SDQ) calculations of HXeCl in single noble-gas layers, and the found order of the H–Xe stretching frequencies ν(Ne) < ν(Xe) < ν(Kr) < ν(Ar) was in agreement with the experiment.[91] The observed H–Kr stretching frequencies of HKrCl (ν(Kr) < ν(Ar)) in Ar and Kr matrices were also successfully simulated. The proposed reason for the "inversed" frequency order ν(Xe) < ν(Kr) < ν(Ar) was the different cage sizes in these matrices. The hybrid quantum-classical simulations performed by Niimi *et al.* were also in agreement with the experimental data for HXeCl, HXeCCH, and HXeBr.[92,93]

1.3 Motivation

The main objectives of this thesis are (i) to identify new noble-gas compounds and (ii) to investigate complexation and matrix effects on selected noble-gas hydrides.

To prepare new noble-gas compounds, FCN and HCCCl are chosen as precursors.[I,II] These precursors are produced by a microwave discharge of gaseous mixtures of $HClC{=}CCl_2$ and $(FCN)_3$ with a noble gas. It is a new approach to prepare matrix-isolated noble-gas compounds.

In the previous experiments with ClCN and BrCN in a Xe matrix, ClXeCN, ClXeNC, and BrXeCN were observed; however, no indication of the corresponding Kr compounds were found in a Kr matrix.[37] The use of fluorine is promising for preparation of the Kr compound FKrCN. Fluorinated Xe cyanides, FXeCN and FXeNC are also expected.

In the previous experiment with HCCF in Kr and Xe matrices, HKrCCF and HXeCCF have been identified.[35] The H–Ng stretching frequencies of these molecules are higher than those of HKrCCH and HXeCCH, respectively,[88,94] featuring a higher stability of the fluorinated species with respect to this coordinate. From this point of view, it is interesting to extend these studies to the HCCCl precursor. In this case, the YNgY' molecules, ClNgCCH, are also possible to observe, similarly to the case of FKrCCH.[35]

HXeI is one of the least stable noble-gas hydrides as judged by the very small dissociation energy (D_0 = 2950 cm^{-1}, experimental value)[95] and the low H–Xe stretching frequency (1193

cm^{-1} in a Xe matrix).[22] It follows that the complexation effect on the properties of HXeI can be very strong; thus, the complexes of this molecule are particularly interesting. Recently, Tsuge *et al*. have studied the complexes of HXeI with HBr and HI.[71] The interaction with HBr is found to induce a larger blue shift of the H–Xe stretching mode (up to +157 cm^{-1}) than the interaction with HI (up to +96 cm^{-1}). Another finding of that work is that the stability of HXeI under broadband IR light of the spectrometer increases upon the complex formation. We intend to expand these data to complexes of HXeI with other molecules to follow the correlation between the interaction strength and the complexation effects. For this purpose, the HXeI···HCl and HXeI···HCCH complexes in a Xe matrix are studied.[III]

The matrix effect on HXeI should be also quite strong due to the weak chemical bonding of this molecule. HXeH is even more specific in this respect because of the absence of the electronegative fragment Y, and the expectations of the matrix effect on this molecule are unclear. It has been suggested that the matrix effect on this molecule should be relatively weak due to its symmetric structure.[90] We investigate HXeI and HXeH in Ar and Kr matrices and compare these results with those in a Xe matrix.[IV] The vibrational properties of these species in different matrices are modeled by hybrid quantum-classical simulations.

2. Methods

2.1 Experimental methods

Matrix isolation is the main experimental tool of this thesis. This technique was invented in order to investigate unstable species, e.g., reactive intermediates and radicals.[11,96-99] The studied species are trapped in an inert solid matrix to extend their lifetime and avoid interaction and reactions with other species. Infrared spectroscopy is widely used to investigate matrix-isolated species. Noble-gases are the most common matrix materials because these substances are transparent in the infrared region and chemically stable although other matrices (e.g., N_2, para-H_2, and CO_2) have also been employed. As mentioned above, matrix isolation has been extensively used to study noble-gas compounds and non-covalent interactions.

In our experiments, gaseous mixtures are deposited at 15–40 K (depending on the matrix gas) onto a CsI window cooled with a closed-cycle helium cryostat (RDK-408D2, Sumitomo Heavy Industries). A typical matrix thickness is ~100 μm. After deposition, the matrix is cooled to the lowest operation temperature (3 K). Photolysis of the matrix is carried out at this temperature by an excimer laser (MSX-250, MPB) at 193 nm (pulse energy density ~10 mJ cm^{-2}), a Kr lamp (Opthos) in the 127–160 nm region, and a Xe lamp (Opthos) in the 150–190 nm region. Then the photolyzed matrix is annealed to mobilize the photolysis fragments, which promotes a desired reaction. The infrared absorption spectra are measured by a Fourier-transform infrared (FTIR) spectrometer (Vertex 80V, Bruker). The secondary irradiation is used to decompose the annealing-induced products typically by a low-pressure mercury lamp (254 nm), an Ar-ion laser (488 nm), and an excimer laser (193 nm).

In the experiments with HCl, HBr, HI, and HCCH, the mixture of the precursor with a matrix gas is prepared by standard manometric procedures and directly deposited to a CsI window.[III,IV] HI was synthesized from 1, 2, 3, 4-tetrahydronaphthalene and iodine as described elsewhere.[100]

In order to prepare the precursors HCCCl and FCN, the microwave discharge method is applied because these species are not available commercially.[I,II] To produce HCCCl, a $HClC{=}CCl_2$/Ng gaseous mixture is discharged in a glass tube by an Evenson cavity and a microwave power supply (SAIREM). The product is a mixture of the matrix gas with HCCCl (main product), HCl, $HClC{=}CCl_2$ (main impurities), ClCCCl, HCCH, C_4H_2, CO_2, CO, and H_2O. This gaseous mixture passes through a trap filled with solid NaOH or Mg turnings (in experiments with deuteration), which eliminates HCl, and the rest of the gas is frozen in the second trap cooled with liquid nitrogen (for Ng = Kr and Xe). To deposit the matrix, the trap is warmed up to −100 ºC (in pentane) to evaporate HCCCl and the noble gas whereas $HClC{=}CCl_2$ and most of other impurities are not evaporated. The HCCCl/Ar mixtures are prepared in a separate vacuum line. A discharged $HClC{=}CCl_2$/Ar (~1/100) gaseous mixture is first frozen at liquid-nitrogen temperature, then HCCCl is evaporated at −100 °C into a glass bulb, and Ar gas is added to make the HCCCl/Ar (~1/1000) mixture. For this preparation method, matrices

contain more CO_2 and H_2O than in the case of Kr and Xe matrices. DCCCl is prepared from $DClC{=}CCl_2$.

To produce FCN, a $(FCN)_3$/Ng (~1/500) gaseous mixture is discharged. The discharge produces a mixture of the matrix gas with FCN, $(FCN)_3$, CO_2, CO, and a small amount of other impurities. This mixture is deposited onto a CsI window without purification.

2.2 Computational methods

Ab initio simulations are performed to support the assignments.[101] These methods are based on solving the time-independent Schrödinger equation:

$$\hat{H}\Psi = E\Psi \tag{1}$$

where $\hat{H}$ is the Hamiltonian operator and E is the energy (eigenvalue) of the stationary state represented by the wave function Ψ (eigenfunction). It is impossible to solve this equation analytically for real molecular systems and various approximations have been employed, including the Born-Oppenheimer and Hartree-Fock approximations. For taking into account the Coulombic electron-electron correlation, the Møller–Plesset perturbation and coupled-cluster theories are often applied. The Møller–Plesset perturbation theory treats the exact Hamiltonian as the summation of the Hatree-Fock Hamiltonian $\hat{H}_0$ and a small perturbation $\hat{V}$:

$$\hat{H} = \hat{H}_0 + \lambda\hat{V} \tag{2}$$

where λ is the dimensionless parameter. The coupled-cluster theory treats the wave function in the form:

$$\Psi = e^T\Phi_0 \tag{3}$$

where Φ_0 is the reference wave function, which is typically a Slater determinant constructed from the Hartree-Fock molecular orbitals.

In Articles I-III, the equilibrium structures, relative energies, and vibrational spectra are calculated at the CCSD(T) and MP2(full) levels of theory.[102,103] The def2-TZVPPD basis set is used for all atoms,[104] and it is taken from the EMSL Basis Set Library using the Basis Set Exchange software.[105] The core electrons of the I and Xe atoms are replaced by an effective potential.[106] The structural optimization and vibrational analysis at the CCSD(T)/def2-TZVPPD level of theory are performed using the MOLPRO program.[107] All calculations at the MP2(full)/def2-TZVPPD level of theory and the natural population analysis at the CCSD/def2-TZVPPD//CCSD(T)/def2-TZVPPD level of theory[108] are performed using the GAUSSIAN 09 program.[109] The vibrational frequencies in this part of work are calculated using the harmonic approximation. For the intermolecular complexes, the interaction energy (E_{int}) is defined as a difference between the total energies of the complexes and of the monomers (with the structures in the complex).[110] While calculating the energy of the complex, the overlap of the wave functions of the complexed monomers induces the basis-set superposition error (BSSE). This error is corrected by the counterpoise (CP) method.[111] In the energetic calculations, the zero-point vibrational energy (ZPVE) is taken into account.

In Article IV, in order to investigate the vibrational spectra of HXeI and HXeH in noble-gas matrices, hybrid quantum-classical simulations are performed by Niimi *et al*. The potential energy term of the Hamiltonian is represented in a pairwise additive form

$$V_{total} = V_{\mathrm{HXeY}} + \sum_{i=1}^{N} V_{\mathrm{HXeY\cdots Ng}_i} + \sum_{i<j}^{N} V_{\mathrm{Ng}_i\cdots\mathrm{Ng}_j} \quad (4)$$

where V_{HXeY} is the potential energy of HXeY (Y = I or H), N is the number of surrounding noble-gas atoms, $V_{\mathrm{HXeY\cdots Ng}}$ and $V_{\mathrm{Ng\cdots Ng}}$ are the interaction potential energy between HXeY and a noble-gas atom and that between two noble-gas atoms. The CCSD(T) method is used to obtain the V_{HXeI}, $V_{\mathrm{HXeI\cdots Ng}}$, $V_{\mathrm{HXeH\cdots Ng}}$, and $V_{\mathrm{Ng\cdots Ng}}$ potentials. For HXeH, the CASPT2 method is used to calculate V_{HXeH} because the CCSD(T) method provides a poor description of the symmetric stretching mode of this molecule at long distances. The cc-pVQZ basis set is used for H and I atoms, and the aug-cc-pVQZ basis set is used for noble-gas atoms (Ar, Kr, and Xe). For Kr, Xe, and I atoms, effective potentials are employed.[106] These calculations are performed using the MOLPRO package.[107] The anharmonic vibrational frequencies of HXeI and HXeH are calculated by the CCSD(T) and CASPT2 methods, respectively. The potential-optimized discrete variable representation (PO-DVR) method[112] is used to calculate the anharmonic vibrational frequencies of HXeY in the presence of surrounding noble-gas atoms. The simulations of the noble-gas hydrides in solid matrices are carried out under periodic boundary conditions, and 500 noble-gas atoms are first placed in a cubic box with the face-centered cubic (*fcc*) lattice. Then, the HXeI and HXeH molecules are inserted into this *fcc* lattice by removing a couple of noble-gas atoms. Three possible orientations in the *fcc* lattice structures are considered for the insertion of HNgY: ⟨100⟩ (four-atomic window), ⟨110⟩ (nearest neighbor), and ⟨111⟩ (three-atomic windows). The number of substituted noble-gas atoms is determined from a sensible choice based on the distance between the adjacent noble-gas atoms along each orientation. After equilibrating the system, a total of 10^7 Monte Carlo steps are taken to obtain statistical averages.

3. New noble-gas compounds

This section focuses on the preparation and identification of new noble-gas compounds in noble-gas matrices using the precursor molecules HCCCl and FCN. The detailed description of these studies can be found in Articles I and II.

3.1 Computational results

3.1.1 Structure and charge distribution

Four groups of noble-gas compounds are studied using the MP2(full) and CCSD(T) methods with the def2-TZVPPD basis set: HNgCCCl, ClNgCCH, FNgCN, and FNgNC (Ng = Ar, Kr, and Xe, see Figure 1). The obtained species are true minima on the potential energy surface and have a linear geometry. Three Ar compounds, HArCCCl, ClArCCH, and FArNC, are obtained at the MP2(full) level of theory, however, they are not found at the CCSD(T) level, which suggests that they are probably unstable.

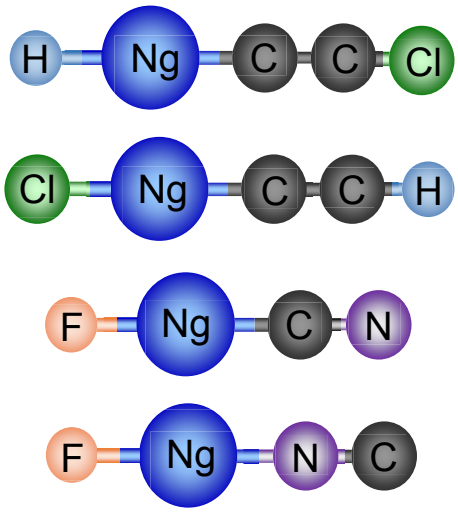


Figure 1. *Calculated structures of HNgCCCl, ClNgCCH, FNgCN, and FNgNC (Ng = Ar, Kr, and Xe). The molecules are linear. The structural parameters are given in Table 1.*

Table 1. *Calculated bond lengths (r, in Å) and partial atomic charges (q, in elementary charges) in HNgCCCl, ClNgCCH, FNgCN and FNgNC (Ng = Ar, Kr, and Xe) at the MP2(full) and CCSD(T) levels of theory with the def2-TZVPPD basis set.*

	MP2(full)			CCSD(T)		
	Ar	Kr	Xe	Ar	Kr	Xe
HNgCCCl						
r(H–Ng)	1.*438*	1.567	1.721	-	1.597	1.748
r(Ng–C(1))	2.160	2.225	2.328	-	2.276	2.361
r(C(1)–C(2))	1.230	1.230	1.231	-	1.226	1.227
r(C(2)–Cl)	1.641	1.640	1.639	-	1.654	1.653
q(H)	+0.177	+0.028	–0.137	-	+0.051	–0.112
q(Ng)	+0.509	+0.644	+0.819	-	+0.629	+0.798
q(C(1))	–0.471	–0.490	–0.531	-	–0.483	–0.524
q(C(2))	–0.289	–0.263	–0.239	-	–0.269	–0.241
q(Cl)	+0.074	+0.081	+0.088	-	+0.072	+0.079
ClNgCCH						
r(Cl–Ng)	2.321	2.399	2.531	-	2.439	2.550
r(Ng–C(1))	2.064	1.984	2.097	-	2.027	2.132
r(C(1)–C(2))	1.221	1.217	1.218	-	1.214	1.216
r(C(2)–H)	1.062	1.062	1.062	-	1.066	1.066
q(Cl)	–0.437	–0.601	–0.653	-	–0.594	–0.651
q(Ng)	+0.578	+0.815	+1.015	-	+0.798	+1.015
q(C(1))	–0.128	–0.268	–0.418	-	–0.249	–0.405
q(C(2))	–0.258	–0.190	–0.184	-	–0.202	–0.199
q(H)	+0.245	+0.244	+0.240	-	+0.247	+0.241
FNgCN						
r(F–Ng)	1.858	1.934	2.041	1.894	1.944	2.036
r(Ng–C)	1.860	1.941	2.089	1.910	1.980	2.128
r(C–N)	1.176	1.174	1.174	1.167	1.166	1.166
q(F)	–0.662	–0.715	–0.768	–0.647	–0.706	–0.758
q(Ng)	+0.807	+0.995	+1.198	+0.787	+0.992	+1.192
q(C)	+0.163	+0.030	–0.103	+0.180	+0.038	–0.093
q(N)	–0.308	–0.310	–0.328	–0.320	–0.324	–0.341
FNgNC						
r(F–Ng)	1.865	1.886	1.994	-	1.902	1.998
r(Ng–N)	1.935	1.954	2.076	-	1.982	2.096
r(N–C)	1.194	1.187	1.185	-	1.187	1.185
q(F)	–0.495	–0.613	–0.701	-	–0.604	–0.696
q(Ng)	+0.914	+1.139	+1.334	-	+1.136	+1.332
q(N)	–0.792	–0.894	–0.997	-	–0.897	–0.994
q(C)	+0.372	+0.368	+0.364	-	+0.365	+0.358

The bond lengths and partial atomic charges of these molecules are shown in Table 1. The bond length related to the noble-gas atom increases with its size. The other bond lengths do not change much in these molecules for different noble-gas atoms. All these molecules exhibit a strong charge-transfer character.[25,35,37] The noble-gas atoms carry large positive charges, and the charge increases with the polarizability of the noble-gas atom. The same noble-gas atoms carry more positive charges in ClNgCCH than in HNgCCCl. In FNgCN and FNgNC, the positive charges of the noble-gas atoms are even larger. Most of the other parts (CCCl in HNgCCCl, Cl and CCH in ClNgCCH, and F and CN in FNgCN and FNgNC) carry negative charges. The H atom is negatively charged in HXeCCCl and positively charged in HArCCCl (MP2(full)) and HKrCCCl. This charge distribution is similar to that in previously investigated HNgCCF, FNgCCH (Ng = Ar, Kr, and Xe), and HalNgCN (Hal = Cl and Br; Ng = Kr and Xe).[35,37]

3.1.2 Energetics

The calculated energies of the investigated compounds are shown in Table 2. The noble-gas compounds are more stable at the MP2(full) level of theory than at the CCSD(T) level. This trend is consistent with the previous conclusion that the MP2 method substantially overestimates the stability of noble-gas hydrides due to an inaccurate description of open-shell species.[34] Thus, we discuss the energetics of the involved species based on the more reliable CCSD(T) results.

Table 2. *Calculated energies (in eV) of the investigated compounds at the MP2(full) and CCSD(T) levels of theory with the def2-TZVPPD basis set.*[a]

	MP2(full)			CCSD(T)		
	Ar	Kr	Xe	Ar	Kr	Xe
HNgCCCl						
HNgCCCl	+0.24	–0.66	–1.51	-	–0.42	–1.38
HCCCl + Ng	–6.10	–6.10	–6.10	–6.05	–6.05	–6.05
ClNgCCH						
ClNgCCH	–0.30	–1.32	–2.43	-	–0.37	–1.57
HCCCl + Ng	–5.55	–5.55	–5.55	–4.75	–4.75	–4.75
FNgCN						
FNgCN	–0.87	–2.13	–3.41	+0.30	–0.83	–2.25
FCN + Ng	–6.37	–6.37	–6.37	–5.28	–5.28	–5.28
FNgNC						
FNgNC	+0.32	–1.00	–2.48	-	+0.12	–1.49
FNC + Ng	–3.09	–3.09	–3.09	–2.22	–2.22	–2.22

[a]For HNgCCCl, ClNgCCH, and FNgCN/FNgNC, the energies are given with respect to the H + Ng + CCCl, Cl + Ng + CCH, and F + Ng + CN asymptotes, respectively. ZPVE is taken into account.

The HNgCCCl, ClNgCCH (Ng = Kr and Xe), FKrCN, FXeCN, and FXeNC molecules are lower in energy with respect to the 3B dissociation asymptotes, which allows their formation at low temperatures. The most stable molecule is FXeCN, which is lower in energy than the F + Ng + CN asymptote by 2.25 eV. Taking into account the expected computational error of the CCSD(T) method,[34] the preparation of ClKrCCH is questionable. FArCN and FKrNC are higher in energy than the 3B asymptote; thus, their experimental observation is improbable. The energies of all optimized molecules are much higher than the 2B dissociation asymptote (HCCCl + Ng or FCN/FNC + Ng). However, the decomposition via this channel is presumably protected by a high energy barrier as it has been discussed for noble-gas hydrides.[25]

3.1.3 Vibrational properties

The calculated vibrational frequencies of HNgCCCl, ClNgCCH, FNgCN, and FNgNC (Ng = Kr and Xe) are given in Table 3. The MP2(full) and CCSD(T) calculations yield similar results. The MP2(full) method is useful because it estimates the transition intensities. Three characteristic frequencies are shown in Table 3 for each molecule.

For the HNgCCCl molecules, the intensity of the H–Ng stretching mode is very high (>1000 km mol^{-1}; MP2(full)), which is characteristic of noble-gas hydrides.[25] The frequencies of this mode are 1421.8 and 1633.0 cm^{-1} for Ng = Kr and Xe at the CCSD(T) level. The C≡C stretching mode of HNgCCCl also has substantial intensity (~100 km mol^{-1}; MP2(full)) to be observed in experiments. The frequency of this mode is lower than that of HCCCl by 29.4 and 29.8 cm^{-1} for Ng = Kr and Xe at the CCSD(T) level. The intensity of the C–Cl stretching mode is about three times lower than that of the C≡C stretching mode. Deuteration strongly decreases the H–Ng stretching frequency whereas the C≡C and C–Cl stretching frequencies do not change much.

For the ClNgCCH molecules, the C–H and C≡C stretching and CCH bending modes have moderate absorptions in the mid-IR region. The C≡C stretching frequencies of ClNgCCH are lower than those of HNgCCCl by 56.8 and 62.6 cm^{-1} for Ng = Kr and Xe at the CCSD(T) level. Deuteration of these molecules significantly decreases the C–H stretching, CCH bending, and C≡C stretching frequencies.

For the FNgCN molecules, the calculated C≡N stretching frequencies are 2159.3, 2185.3, and 2191.8 cm^{-1} (Ng = Ar, Kr, and Xe) at the CCSD(T) level, which are lower than that of FCN (2342.8 cm^{-1}). The C≡N stretching frequencies of FNgNC are lower than that of FNC (2155.5 cm^{-1}) as well. The MP2(full) method predicts similar results for the frequencies and estimates the transition intensities. For FNgCN, the F–Ng stretching mode has the strongest intensity (>200 km mol^{-1}) while the Ng–C stretching mode is the weakest. For FNgNC, the C≡N stretching mode is the strongest while the Ng–N stretching mode is the weakest. The intensities of the F–Ng stretching mode of FNgCN and FNgNC are similar.

Table 3. *Calculated characteristic vibrational frequencies (in cm^{-1}) and absorption intensities (in km mol^{-1}, in parentheses) of HNgCCCl, ClNgCCH, FNgCN and FNgNC (Ng = Kr and Xe) at the MP2(full) and CCSD(T) levels of theory with the def2-TZVPPD basis set.*[a]

	MP2(full)		CCSD(T)	
Assignment	Kr	Xe	Kr	Xe
HNgCCCl				
ν_{H-Ng}	1659.3 (2502.5) *1179.0 (1273.3)*	1744.9 (1450.9) *1238.3 (729.1)*	1421.8 *1010.6*	1633.0 *1158.8*
$\nu_{C\equiv C}$	2073.4 (80.7) *2073.3 (71.1)*	2069.8 (95.9) *2069.8 (97.3)*	2122.5 *2122.7*	2122.1 *2123.0*
ν_{C-Cl}	809.0 (28.0) *808.8 (33.6)*	810.7 (29.6) *810.4 (33.5)*	782.5 *784.4*	787.3 *789.2*
ClNgCCH				
ν_{C-H}	3480.5 (80.9) *2676.8 (26.0)*	3479.6 (80.2) *2676.9 (31.2)*	3443.9 *2662.4*	3443.0 *2661.3*
$\nu_{C\equiv C}$	2030.9 (68.4) *1908.5 (102.1)*	2041.0 (36.2) *1918.4 (61.6)*	2059.5 *1925.7*	2065.7 *1932.8*
CCH bend	743.1 (35.5) *577.0 (16.1)*	756.3 (35.6) *590.3 (15.3)*	677.6 *522.6*	684.2 *529.7*
FNgCN				
ν_{F-Ng}	529.9 (273.1)	499.3 (220.3)	505.8	496.1
ν_{Ng-C}	388.5 (37.6)	402.2 (53.8)	357.4	384.0
$\nu_{C\equiv N}$	2076.6 (114.3)	2083.8 (71.8)	2185.3	2191.8
FNgNC				
ν_{F-Ng}	564.8 (269.4)	533.9 (222.9)	528.7	524.4
ν_{Ng-N}	389.7 (20.7)	409.7 (84.9)	355.0	397.1
$\nu_{N\equiv C}$	2028.2 (342.3)	2044.1 (315.5)	2050.8	2069.4

[a]The results for the deuterated species DNgCCCl and ClNgCCD are presented in italics.

3.2 Experimental results

3.2.1 HKrCCCl and HXeCCCl

The IR spectra of HCCCl/Ng (Ng = Kr and Xe) matrices are shown in Figure 2. Small amounts of C_4H_2,[113] CO_2, CO, H_2O,[114,115] HCCH,[116] and ClCCCl[117] are present in the matrices as impurities. The HCCCl/Ng gaseous mixtures were obtained by a microwave discharge and purification of $HClC{=}CCl_2$/Ng mixtures as described in Section 2.

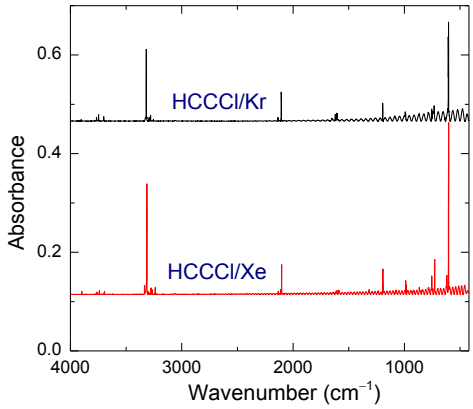


Figure 2. *FTIR spectra of HCCCl in Kr and Xe matrices. Weak bands of H_2O, CO, HCCH, and ClCCCl can be seen in the spectra. The sinusoidal background is due to interference of light. The spectra are measured at 3 K.*

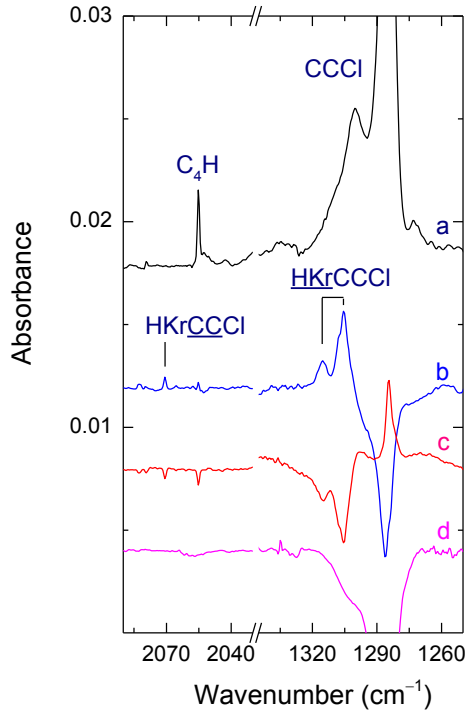


Figure 3. *HKrCCCl in a Kr matrix. The difference FTIR spectra show the results of (a) Kr-lamp photolysis of a HCCCl/Kr matrix; (b) annealing of the previous matrix at 35 K for 5 min; (c) irradiation of the previous matrix by a mercury lamp (254 nm); (d) Kr-lamp photolysis and annealing at 20 K of a HCCCl/Ar matrix. The deposition temperatures are 20 and 15 K for Kr and Ar matrices, respectively. The sinusoidal interference patterns are subtracted. The spectra are measured at 3 K.*

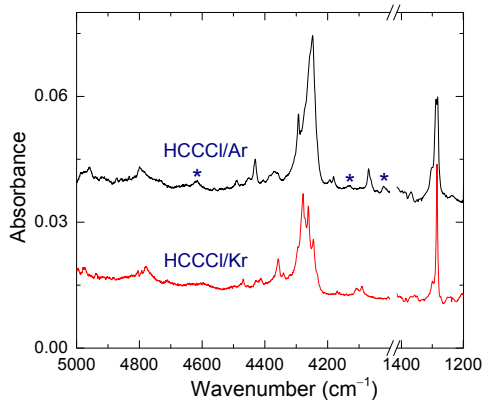


Figure 4. *Difference FTIR spectra showing the result of photolysis of HCCCl in Ar and Kr matrices. The strongest bands are assigned to the CCCl radical. The bands of the CCH radical are marked with asterisks.*[126] *The sinusoidal interference patterns are subtracted. The spectra are measured at 3 K.*

Table 4. *Experimental frequencies (in cm^{-1}) of HKrCCCl and HXeCCCl.*

Assignm	HKrCCCl	DKrCCCl	HXeCCCl	DXeCCCl
$\nu_{H(D)-N}$	1306, 131	970, 980	1500,[a] 1550, 1569	)89,[a] 1122, 1135
$\nu_{C\equiv C}$	2070.7	2070.3	2077.4	2077.5

[a] Unstable configuration.

Kr-lamp photolysis for 5 h decomposes ~20% of HCCCl in a Kr matrix, and further decomposition is probably limited by photolysis-induced absorbers (self-limitation of photolysis).[118] The known products of the photolysis are $(KrHKr)^+$,[119,120] CO_2, CO, C_4,[121] C_4H radicals (spectrum a in Figure 3),[113,122] and CCH radicals.[94] In a Xe matrix, 193-nm photolysis of HCCCl is found to be more efficient than Kr-lamp photolysis. Typically, 5000 pulses at 193 nm decomposes ~20% of HCCCl. The known photolysis products include $(XeHXe)^+$,[123] C_4,[113] ClCO,[124] CO_2, CO, and Xe–CC.[125] In addition to the known species, UV photolysis in Ar and Kr matrices produces bands at ~1285 and 3373 cm^{-1} and a number of bands in the 4000–5000 cm^{-1} region that are assigned to the CCCl radical (Figures 3 and 4). These bands in a Xe matrix are much weaker, which is probably due to efficient photodecomposition of CCCl.

Annealing of a photolyzed matrix at ~30 K (Kr) and at ~40 K (Xe) mobilizes H atoms[127-129] and leads to the formation of new noble-gas compounds HKrCCCl in a Kr matrix (spectrum b in Figure 3) and HXeCCCl in a Xe matrix (spectrum a in Figure 5) via the H + Ng + CCCl (Ng = Kr and Xe) reaction. The absorption frequencies of HKrCCCl and HXeCCCl are given in Table 4. The known annealing-induced products are C_4H[113,122] and HKrCCH[94] in a Kr matrix

and HXeH,[23] HXeCl,[22] HXeCC,[88] HXeCCH,[88] HXeO,[130] and C_4H[113] in a Xe matrix. For HXeCCCl, three H–Xe stretching bands at 1500 cm^{-1}, 1550, and 1568 cm^{-1} are observed after annealing at 40 K. Annealing at higher temperature (≥43 K) leads to a decrease of the 1500 cm^{-1} band and to an increase of the 1550 and 1568 cm^{-1} bands (spectrum b in Figure 5). The experiments with DCCCl produce DKrCCCl in a Kr matrix and DXeCCCl in a Xe matrix (Table 4). The bands assigned to HKrCCCl and HXeCCCl can be easily bleached by UV light similar to other noble-gas hydrides (spectra c in Figures 3 and 5). The bands assigned to CCCl decrease in intensity upon annealing and increase upon decomposition of HNgCCCl molecules, which evidently supports the assignment. No bands suitable for ClKrCCH and ClXeCCH are detected in these experiments. In a HCCCl/Ar matrix, no bands near the absorptions of HKrCCCl and HXeCCCl are observed after photolysis and annealing (spectrum d in Figure 3). Bands suitable for HArCCCl and ClArCCH are not observed either.

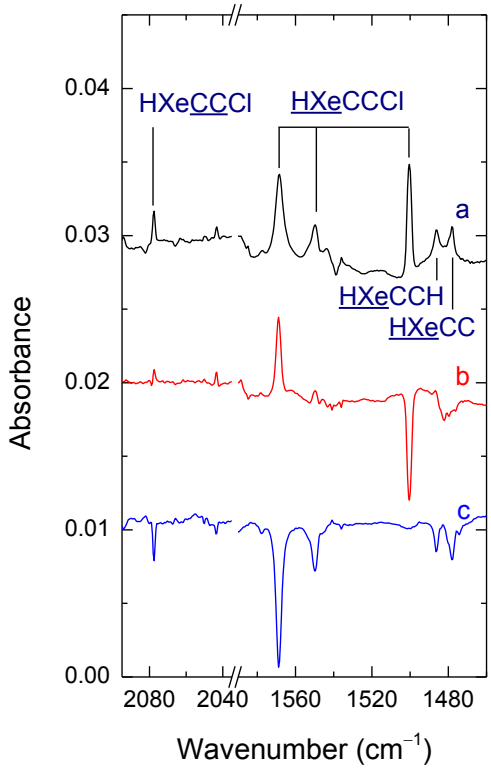


Figure 5. *HXeCCCl in a Xe matrix. The difference FTIR spectra show the results of (a) annealing at 40 K for 5 min; (b) annealing of the previous matrix at 50 K for 5 min; (c) irradiation at 193 nm (100 pulses) of the previous matrix. Prior to the first annealing, the HCCCl/Xe matrix is photolyzed by 193-nm light. The deposition temperature is 30 K. The sinusoidal interference patterns are subtracted. The spectra are measured at 3 K.*

3.2.2 FKrCN, FXeCN, and FXeNC

For deposition of a $(FCN)_3$/Ng (Ng = Kr and Xe) gas mixture with a microwave discharge, the spectrum of the matrix is dominated by FCN and non-decomposed $(FCN)_3$ (Figure 6). Some impurities (NCCN ,[131] HCN,[132] CO, CO_2, CO-water complex,[133] and monomeric water) are also observed.

Photolysis by a Xe lamp for 60 min decomposes 20–30% of FCN in Kr and Xe matrices. Three new new noble-gas compounds, FKrCN in a Kr matrix (spectrum a in Figure 7) and FXeCN and FXeNC in a Xe matrix (spectrum a in Figure 8), are produced by the photolysis. The experimental frequencies of FKrCN, FXeCN, and FXeNC are shown in Table 5. A number of known species are also generated by the photolysis, e.g., NCNC,[134] FNC,[135] CN radical (in a Kr matrix),[136,137] and $(NgHNg)^+$.[119,120] The amount of $(FCN)_3$ does not change much upon Xe-lamp photolysis.

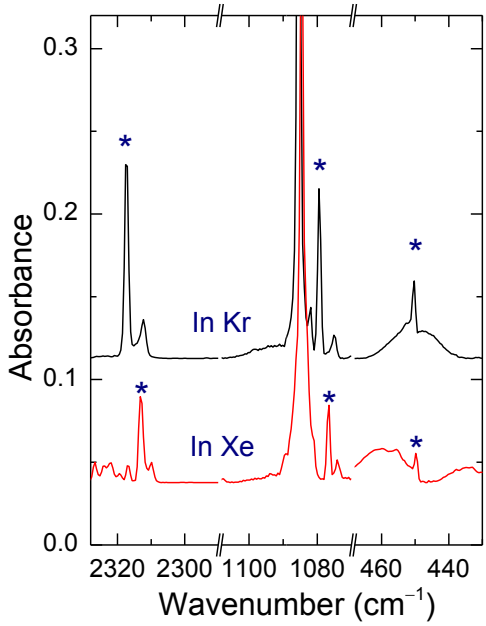


Figure 6. *FTIR spectra of matrices prepared from discharged $(FCN)_3$/Ng (Ng=Kr and Xe) gaseous mixtures. The bands of FCN are marked with asterisks. Other bands originate from $(FCN)_3$. The deposition temperatures are 25 K and 35 K for Kr and Xe matrices, respectively. The spectra are measured at 3 K.*

Table 5. *Experimental frequencies (in cm^{-1}) of FNgCN and FNgNC (Ng = Kr and Xe)*

	FNgCN	
Assignment	Kr	Xe
ν_{F-Ng}	505	487
ν_{Ng-C}	357	366
$\nu_{C\equiv N}$	2158	2159
	FNgNC	
	Kr	Xe
ν_{F-Ng}	-	517
ν_{Ng-N}	-	-
$\nu_{N\equiv C}$	-	2041

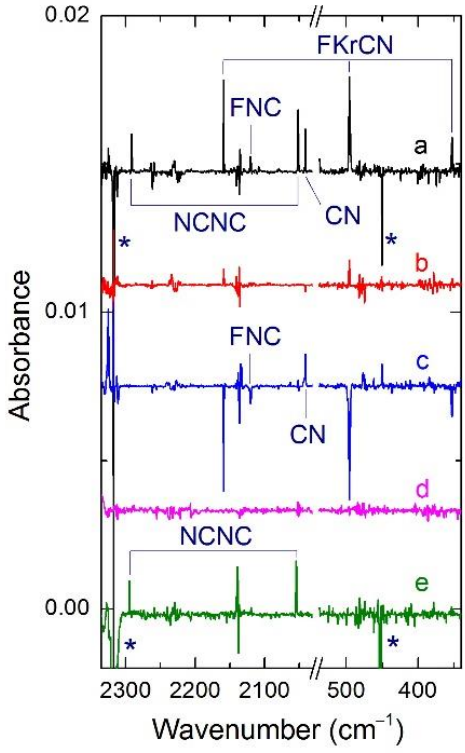


Figure 7. *FKrCN in a Kr matrix. The difference FTIR spectra show the results of (a) Xe-lamp photolysis of a FCN/Kr matrix; (b) annealing at 25 K of the previous matrix; (c) irradiation at 193 nm of the previous matrix; (d) Xe-lamp photolysis and annealing at 25 K of a (FCN)$_3$/Kr gas mixture without discharge; (e) Xe-lamp photolysis and annealing at 20 K of a FCN/Ar matrix. The bands of FCN are marked with asterisks. The deposition temperatures are 25 and 15 K for Kr and Ar matrices. The spectra are measured at 3 K.*

Upon annealing at ~20 K, the bands of FKrCN in a Kr matrix somewhat increase in intensity and the amount of CN decreases (spectrum b in Figure 7). No bands suitable for FKrNC is observed upon photolysis and annealing. In a Xe matrix, the bands of FXeCN and FXeNC substantially increase upon annealing at 6–10 K (spectrum b in Figure 8). Short irradiation at 193 nm efficiently decomposes these species (spectra c in Figures 7 and 8). For deposition of a $(FCN)_3$/Ng (Ng = Kr and Xe) mixture without discharge (spectra d in Figures 7 and 8) and a $(FCN)_3$/Ar mixture with discharge (spectrum e in Figure 7), no bands near the absorptions of FKrCN, FXeCN, and FXeNC are observed after photolysis and annealing.

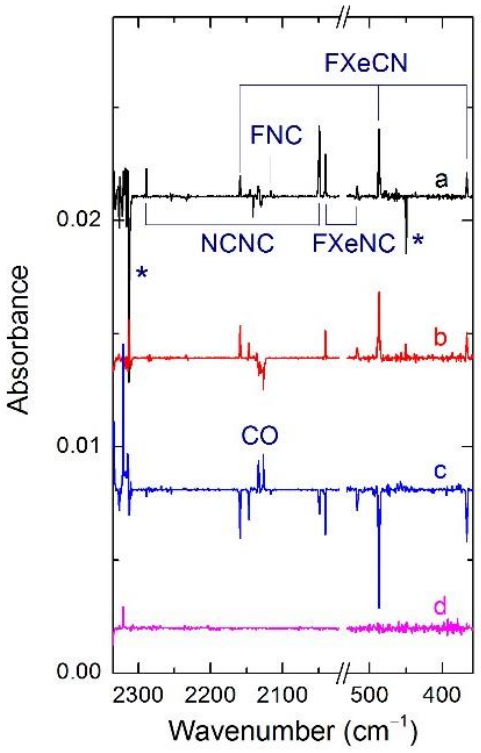


Figure 8. *FXeCN and FXeNC in a Xe matrix. The difference FTIR spectra show the results of (a) Xe-lamp photolysis of a FCN/Xe matrix; (b) annealing at 10 K of the previous matrix; (c) irradiation at 193 nm of the previous matrix; (d) Xe-lamp photolysis and annealing at 10 K of a $(FCN)_3$/Xe (without discharge). The bands of FCN are marked with asterisks. The deposition temperature is 35 K. The spectra are measured at 3 K.*

3.3 Discussion

In this section, five new noble-gas compounds are described. The first type of the compounds belongs to noble-gas hydrides: HKrCCCl in a Kr matrix and HXeCCCl in a Xe matrix. These

compounds are synthesized by UV photolysis of HCCCl/Ng matrices to form the H + CCCl fragments and annealing the matrices to mobilize the H atoms and to promote the H + Ng + Y → HNgY reaction.[25] The HCCCl molecules are produced by a microwave discharge of HClC=CCl_2/Ng gaseous mixtures.

The assignment of these noble-gas hydrides are fully supported by the *ab initio* calculations. For example, the change of the experimental C≡C stretching frequency from HCCCl to HKrCCCl (–35 cm^{-1}) is in good agreement with the calculated value (–29.4 cm^{-1} (CCSD(T)). The C≡C stretching frequency of HKrCCCl is theoretically (MP2(full)) 101.7 cm^{-1} smaller than that of HKrCCF (MP2),[35] similarly to the experimental difference of 106.3 cm^{-1}. The H–Kr stretching frequency is somehow overestimated (CCSD(T): 1421.8 cm^{-1}; experiment: 1315 and 1306 cm^{-1}), which is mainly due to the use of the harmonic approximation.[138] The H–Kr stretching frequency order for HKrCCX (X = F, Cl, and H) molecules is 1384 cm^{-1} (HKrCCF)[35] > 1315 and 1306 cm^{-1} (HKrCCCl) > 1241.5 cm^{-1} (HKrCCH),[94] which agrees with the calculations (1694.2 cm^{-1} (HKrCCF)[35] > 1659.3 cm^{-1} (HKrCCCl) > 1575 cm^{-1} (HKrCCH)[94]). The intensity ratio of the 2070.7 and 1306/1315 cm^{-1} experimental bands (0.02) is in good agreement with the calculations (0.03; MP2(full)). In the deuteration experiments, DKrCCCl is observed. The H/D frequency ratio of the H–Kr stretching mode of HKrCCCl (1.344) is similar to that of HKrCCH (1.350)[94] and somewhat smaller than that of HKrCCF (1.370).[35]

For HXeCCCl, the calculated and experimental spectra are also in good agreement (Tables 3 and 4). The temperature transformation of the H–Xe stretching bands of HXeCCCl in a Xe matrix is an interesting observation. The lower-frequency band (1500 cm^{-1}) decreases in intensity upon annealing above 43 K whereas the higher-frequency bands (1550 and 1568 cm^{-1}) increase (spectrum b in Figure 5). This behavior is presumably connected with temperature-induced changes of the local matrix morphology around the embedded HXeCCCl molecule. A similar phenomenon was reported for HArF in an Ar matrix and for HKrF in a Kr matrix.[139, 140] This process was studied in more detail for HArF and explained by temperature-induced mobility of a vacancy in the vicinity of the embedded molecule.[141] Similar temperature behavior is observed for the three bands of DXeCCCl (1089 (unstable), 1122 (stable), and 1135 (stable) cm^{-1}). Remarkably, the H/D frequency ratio for these three bands increases with the H(D)–Xe stretching frequency (1.377, 1.381, and 1.382), which indicates an increase of the harmonicity of the H–Xe stretching mode with the frequency. In addition, these H/D frequency ratios of HXeCCCl are very close to the corresponding values for HXeCCH (1.379)[88] and HXeCCF (1.380).[35]

For the H–Xe stretching mode, the computational order of the frequencies (1759.4 cm^{-1} (HXeCCF)[35] > 1744.9 cm^{-1} (HXeCCCl) > 1736 cm^{-1} (HXeCCH)[88]) agrees with the experiment (1548 cm^{-1} (HXeCCF)[35] > 1500 cm^{-1} (HXeCCCl) > 1486.4 cm^{-1} (HXeCCH)[88]) only if we use the unstable band of HXeCCCl. The stable bands of HXeCCCl (1550 and 1568

cm^{-1}) are higher in frequency than that of HXeCCF (1548 cm^{-1}).[35] This observation suggests that the matrix arrangement around HXeCCCl in the stable configuration is different from those around HXeCCH and HXeCCF.

The second type of the new noble-gas compounds include FKrCN in a Kr matrix and FXeCN and FXeNC in a Xe matrix (fluorinated noble-gas cyanides). The synthesis of these molecules includes photolysis of the precursor (FCN) in noble-gas matrices to form the F + CN fragments and annealing of the matrices to mobilize F atoms and to promote the F + Ng + CN $\rightarrow$ FNgCN /FNgNC reaction. As a difference from the previous case, these molecule are formed already upon photolysis, which indicates the locality of this process.[37] In some cases, the HNgY molecules are also produced by UV photolysis (HXeNCO, HArF, HKrCl, and HXeBr).[24,69,142,143]

The assignment of the fluorinated noble-gas cyanides is solid. The change of the C≡N stretching frequency from FCN to FKrCN is −157.5 cm^{-1} (CCSD(T)) and −159 cm^{-1} (experiment). The experimental F−Kr and Kr−C stretching frequencies of FKrNC are also in agreement with the calculations (Tables 3 and 4). In addition, the intensity order of the 505 (the strongest), 2158, and 357 (the weakest) cm^{-1} experimental bands is also predicted (MP2(full)).

The difference of the C≡N stretching frequency between FCN and FXeCN is −151.0 cm^{-1} (CCSD(T)) and −158 cm^{-1} (experiment) whereas for FNC and FXeNC, this difference is −86.1 cm^{-1} (CCSD(T)) and −79 cm^{-1} (experiment). The change of the F−Xe stretching frequencies from FXeCN to FXeNC is −28.3 cm^{-1} (CCSD(T)) and −30 cm^{-1} (experiment) and the corresponding values for the C≡N stretching mode are +122.4 cm^{-1} and +118 cm^{-1}. The experimental C≡N stretching frequency of FXeCN (2159 cm^{-1}) is higher than those of ClXeCN (2145 cm^{-1}) and BrXeCN (2139 cm^{-1}).[37] The same trend is observed for FXeNC (2041 cm^{-1}) and ClXeNC (2030 cm^{-1}). The calculations predict the same C≡N stretching frequency order for these species. Thus, the C≡N stretching frequency of these compounds increases with the electronegativity of the halogen atom.

Ar compounds (HArCCCl, ClArCCH, FArCN, and FArNC) are not found in these experiments, which agrees with the calculated energetics (Table 2). No bands suitable for FKrNC are observed either, which is also consistent with the calculations (Table 2). The non-observation of ClKrCCH in a Kr matrix may also be connected with the lack of its energetic stability and/or with a minor amount of Cl atoms produced by UV photolysis of HCCCl. The latter explanation is consistent with the absence of HKrCl after annealing. The nonappearance of ClXeCCH in a Xe matrix is more surprising. This species is energetically stable (Table 2) and should be presumably formed in the Cl + Xe + CCH reaction upon photolysis and/or annealing. The presence of some amounts of CCH and Cl is justified by the formation of HXeCCH and HXeCl upon annealing of the photolyzed matrices. The lack of the observation of ClXeCCH can be explained in two ways. The first reason is low concentrations of CCH and Cl, which are insufficient to produce measurable amounts of ClXeCCH. HXeCCH and HXeCl

are detected by the very strong H–Xe stretching mode (>1000 km mol^{-1}).[116,22] For ClXeCCH, the intensities of the characteristic transitions are much lower. Thus, if the concentration of ClXeCCH is small, it is unlikely to be observed. The second possible reason is that the Cl atoms originate from photodecomposition of CCCl radicals whereas CCH radicals are mainly produced by photolysis of HCCH (not from HCCCl). In this case, the formation of ClXeCCH needs extensive thermal mobility of Cl atoms in a Xe matrix, which is questionable.

In these experiments, we have obtained the IR spectrum of the CCCl radical. Tarroni *et al.* reported the *ab initio* IR spectrum of CCCl with strong absorptions in the 1250–1450, 3350–3450, and 4000–5000 cm^{-1} spectral regions with intensities up to ~7000 km mol^{-1}.[144] The experimental spectra of CCCl are in good agreement with those calculations. After photolysis of HCCCl in an Ar matrix, bands at 1282/1288 and 3357 cm^{-1} as well as several bands in the 4000–5000 cm^{-1} region are observed, and similar bands appear in Kr (Figure 4) and Xe (with much weaker intensity) matrices. To remind, the CCF spectrum was reported by Tarroni *et al.* upon photolysis of HCCF in Ar and Kr matrices and supported by the calculations.[145]

4 Environmental effects

In this section, the computational and experimental studies of the HXeI···HY (Y = Cl and CCH) complexes and of the matrix effects on HXeI and HXeH are described. Comparison with the previous results on similar systems is presented. The detailed description of these studies can be found in Articles III and IV.

4.1 Complexes of HXeI

4.1.1 Computational results

The CCSD(T) and MP2(full) methods are used to calculate the equilibrium structures, relative energies, and vibrational spectra of the HXeI···HY (Y = Cl and CCH) complexes (see Section 2 for computational details).

For the HXeI···HCl complex, four structures are obtained at the MP2(full)/def2-TZVPPD level of theory whereas structure C is not found by the CCSD(T) method (Tables 6 and Figure 9). Structure D has positive interaction energy at both levels of theory. For the HXeI···HCCH complex, the MP2(full) method gives two structures (A and C); however, only structure A is obtained at the CCSD(T) level (Table 6 and Figure 9). Based on these results, in the following, we only consider structures A and B for the HXeI···HCl complex and structure A for the HXeI···HCl complex.

The partial atomic charges are shown in Table 7. For structure A, the charge of the HXe group increases by +0.059*e* and by +0.039*e* upon complexation (CCSD) for HXeI···HCl and HXeI···HCCH, respectively. In structure B of the HXeI···HCl complex, the complexation effect on the atomic charges is rather weak. HCl and HCCH in the complexes carry negative charges.

Table 6. *BSSE-corrected interaction energies of the HXeI···HCl and HXeI···HCCH complexes (in kcal mol^{-1}).*[a]

	Structure A	Structure B	Structure C	Structure D
HXeI···HCl				
CCSD(T)	−4.94 (−3.72)	−0.98 (−0.28)	···	+0.31 (+1.03)
MP2(full)	−6.40 (−4.55)	−1.81 (−0.36)	−1.35 (−0.20)	+0.65 (+1.04)
HXeI···HCCH				
CCSD(T)	−3.10 (−2.67)	···	···	···
MP2(full)	−3.86 (−1.79)	···	−2.31 (−0.19)	···

[a] Interaction energies additionally corrected by the difference of ZPVEs between the complex and monomers (E_{int}^{CP} + ΔZPVE) are given in parentheses. The complex structures are shown in Figure 9.

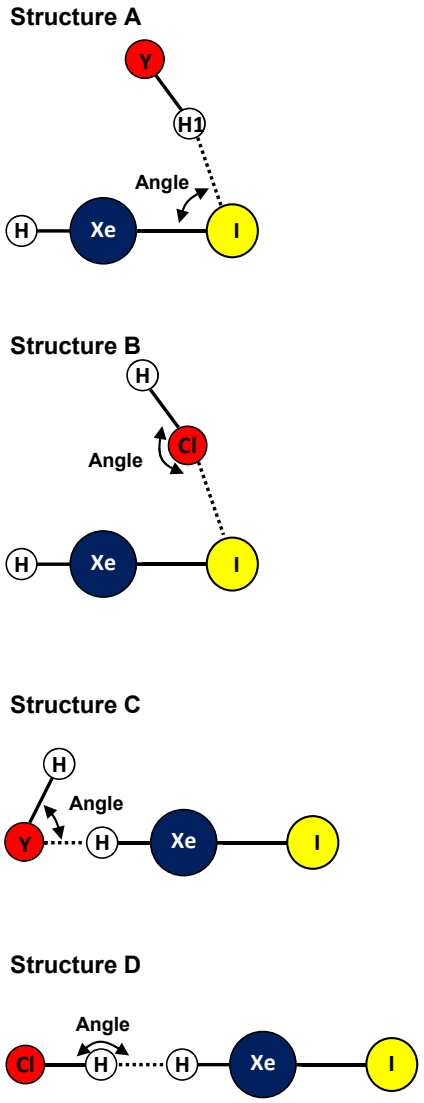


Figure 9. *Structures of the HXeI···HY (Y=Cl and CCH) complexes. The interaction energies are given in Table 6. The selected structural parameters are given in Table 7. Structure C of the HXeI···HCCH complex at the MP2(full) level is T-shaped (C_{2v} symmetry).*

The structural parameters are shown in Table 7. For the HXeI···HCl complex (structure A), the H–Xe bond is substantially shortened and the Xe–I bond is lengthened compared to monomeric HXeI. The HCl bond becomes longer in this structure. In structure B of this complex, the bond lengths of HXeI and HCl are not changed much upon complexation. In the HXeI···HCCH complex (structure A), the H–Xe bond length becomes shorter and the Xe–I

Table 7. *Selected structural parameters and partial atomic charges (in elementary charges) for the HXeI···HCl and HXeI···HCCH complexes optimized at the CCSD(T) and MP2(full) levels of theory with the def2-TZVPPD basis set.*[a,b]

	Structure	$r(H_{HXeI}–Xe)$	r(Xe–I)	r(interm)	r(H–Cl)	angle	$q(H_{HXeI})$	q(Xe)	q(I)
CCSD(T)	**HXeI and HCl monomers**								
		1.768	3.024	···	1.275	···	−0.003	+0.643	−0.640
	HXeI···HCl complexes								
	A	1.730	3.055	2.651	1.296	72.1	+0.034	+0.665	−0.664
	B	1.763	3.024	4.111	1.279	62.7	−0.005	+0.649	−0.643
	D	1.797	3.009	2.143	1.277	180.0	+0.034	+0.665	−0.640
	HXeI···HCCH complexes								
	A	1.744	3.041	3.073	···	70.2	+0.018	+0.661	−0.670
MP2(full)	**HXeI and HCl monomers**								
		1.709	2.975	···	1.269	···	−0.022	+0.678	−0.656
	HXeI···HCl complexes								
	A	1.677	3.012	2.495	1.296	71.8	+0.017	+0.699	−0.661
	B	1.700	2.974	3.829	1.271	66.4	−0.021	+0.686	−0.659
	C	1.692	2.993	2.679	1.271	180.0	+0.015	+0.672	−0.699
	D	1.728	2.944	1.993	1.272	180.0	−0.083	+0.689	−0.602
	HXeI···HCCH complexes								
	A	1.689	2.992	2.904	···	69.2	0.000	+0.695	−0.679
	C	1.686	3.017	2.346	···	90[c]	+0.047	+0.659	−0.737

[a]The bond lengths are in Ångströms and the angles are in degrees. The partial atomic charges in the CCSD(T) row are calculated by the CCSD method.[108]

[b] r(interm) is shown by dotted lines in Figure 9.

[c]Structure C of the HXeI···HCCH complex is T-shaped (C_{2v} symmetry).

bond length becomes longer with respect to monomeric HXeI. The structure of the HCCH moiety is not changed significantly. The HXeI molecule is slightly bent in these complexes.

The calculated frequencies are presented in Table 8. For the HXeI···HCl complex, the complexation-induced shift of the H–Xe stretching mode is +166.7 cm^{-1} for structure A at the CCSD(T) level of theory. For structure B, this shift is much smaller (+19.5 cm^{-1}). For the HXeI···HCCH complex (structure A), the monomer-to-complex shift of the H–Xe stretching mode is +103.5 cm^{-1} (CCSD(T)). The H–Xe stretching intensities decrease in these complexes with respect to the HXeI monomer.

In the HXeI···HCl complex, the monomer-to-complex shift of the HCl stretching frequency is −265.6 cm^{-1} in structure A (CCSD(T)). The absorption intensity of this mode strongly increases to ~1000 km mol^{-1} (MP2(full)), which is comparable to the intensity of the H–Xe stretching mode of HXeI. For structure B, the change of the HCl vibration is much weaker. For the HXeI···HCCH complex, the change of the vibrational properties of HCCH is also not

Table 8. *Calculated characteristic vibrational frequencies (in cm^{-1}) and monomer-to-complex shifts (in brackets, in cm^{-1}) of the HXeI···HCl and HXeI···HCCH complexes at the CCSD(T) and MP2(full) levels of theory with the def2-TZVPPD basis set.*[a]

	Monomer	Structure A	Structure B	Structure C	Structure D
HXeI···HCl					
CCSD(T)	1327.2	1493.9 [+166.7]	1346.7 [+19.5]	···	1228.8 [−98.4]
MP2(full)	1662.6 (2791)	1788.8 [+126.2] (2091)	1678.4 [+15.8] (2630)	1733.7 [+71.1] (1483)	1542.2 [−120.4] (4473)
HXeI···HCl					
CCSD(T)	3007.3	2741.7 [−265.6]	2974.4 [−32.9]	···	2965.2 [−42.1]
MP2	3070.0 (52)	2683.7 [−386.3] (1033)	3049.9 [−20.1] (32)	3053.2 [−16.8] (76)	3004.9 [−65.1] (517)
HXeI···HCCH					
CCSD(T)	1327.2	1430.7 [+103.5]	···	···	···
MP2(full)	1662.6 (2791)	1732.7 [+70.1] (2366)	···	1755.5 [+92.9] (369)	···
HXeI···HCCH					
CCSD(T)	3406.6	3364.9 [−41.7]	···	···	···
MP2(full)	3445.3 (95)	3376.2 [−69.1] (200)	···	3428.5 [−16.8] (114)	···
HXeI···HCCH					
CCSD(T)	1996.6	1987.8 [−8.8]	···	···	···
MP2(full)	1977.4 (0.0)	1960.9 [−16.5] (5)	···	1969.0 [−8.4] (21)	···
HXeI···HCCH (bend)					
CCSD(T)	749.2[b]	762.3 [+13.1] 766.9 [+17.7]	···	···	···
MP2(full)	767.1[b] (89)	792.5 [+25.4] (55) 797.2 [+30.1] (113)	···	771.3 [+4.2] (81) 793.7 [+26.6] (196)	···

[a]The infrared intensities (in km mol^{-1}) calculated by the MP2(full) method are shown in parentheses.
[b]Doubly degenerate.

significant. The intensities of the characteristic transitions of HCCH in the complex are much smaller than that of the H–Xe stretching mode of HXeI. Therefore, the experimental observation of these modes is questionable.

4.1.2 Experimental results

In a HI/Xe matrix, several HI monomer bands are observed after deposition (the strongest band at 2214 cm^{-1}).[146] Addition of HCl to a HI/Xe matrix leads to the formation of two complexes, the HCl···HI (2190 and 2187 cm^{-1}, HI acts as a proton donor) and HI···HCl complex (2785 cm^{-1},

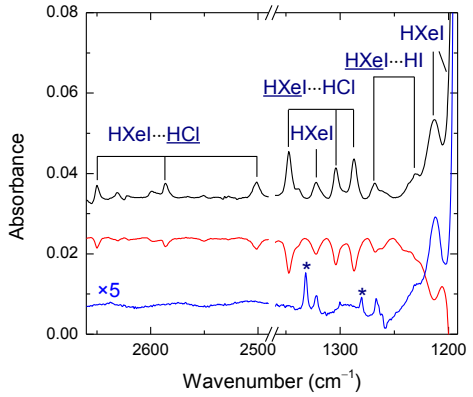


Figure 10. *HXeI···HCl* complex in a Xe matrix. *FTIR difference spectra of a HI/HCl/Xe matrix showing the results of annealing at 60 K after 193-nm photolysis (top spectrum) and irradiation of the annealed matrix by a mercury lamp (middle spectrum). FTIR difference spectrum of a HI/Xe matrix showing the result of annealing at 60 K after 193-nm photolysis (bottom spectrum). The bands marked with asterisks are from HXeI···H_2O induced by H_2O impurity in the matrix.*[72] *The spectra are measured at 3 K.*

HCl acts as a proton donor). Addition of HCCH to a HI/Xe matrix produces the HCCH···HI (2175 cm^{-1}, T-shaped, HI acts as a proton donor) complex. The HI···HCCH complex (linear) is probably not formed because it is energetically unstable.[III] After 300 pulses of 193-nm light, more than 80% of HI is decomposed whereas the decomposition of HCl and HCCH is much less efficient. The ionic species such as $(ClHCl)^-$, $(IHI)^-$, and $(XeHXe)^+$ are observed after photolysis.[123,147] No bands of the I···HCl and I···HCCH complexes are found after photolysis of the HI/HCl/Xe and HI/HCCH/Xe matrices.

Annealing at ~40 K mobilizes H atoms in a Xe matrix,[128,129] which allows the formation of noble-gas hydrides. In the HI/HCl/Xe matrices, annealing-induced bands at 1287, 1304, 1348, 2501, 2586, and 2651 cm^{-1} are assigned to the HXeI···HCl complex (Figure 10). The known species observed after annealing include HXeI,[22] HXeH,[23] and HXeCl.[22] In the HI/HCCH/Xe matrices, the HXeI···HCCH complex (1242 cm^{-1} with a weaker band at 1248 cm^{-1}, Figure 11) is found after photolysis and annealing. HXeI,[22] HXeH,[23] $HCCH_2$,[148] HXeCCH,[29, 88] HXeCC,[88] and HXeCCXeH[88] are also observed. No indications of the HXeCl···HI and HXeCCH···HI complexes are found. The bands assigned to the HXeI···HCl and HXeI···HCCH complexes can be easily bleached by UV and visible light (Figures 10 and 11). The H–Xe stretching frequencies of these complexes are shown in Table 9.

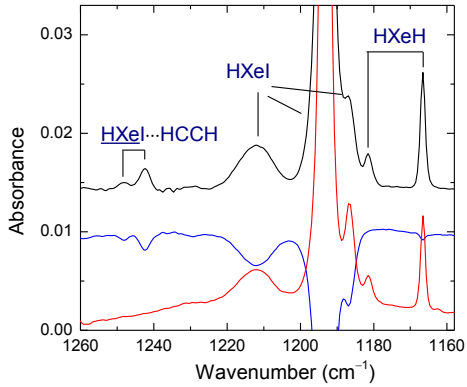


Figure 11. *HXeI···HCCH complex* in a Xe matrix. *FTIR difference spectra of a HI/HCCH/Xe matrix showing the results of annealing at 60 K after 193-nm photolysis (top spectrum) and irradiation of the annealed matrix by a 488-nm laser (middle spectrum). FTIR difference spectrum of a HI/Xe matrix showing the result of annealing at 60 K after 193-nm photolysis (bottom spectrum). The spectra are measured at 3 K.*

Table 9. *Experimental H–Xe stretching frequencies (in cm^{-1}) of the HXeI···HY (Y = Cl, Br, I, and CCH) complexes* [a]

Species	Frequency	Structure
HXeI···HCl	1287 (+94)	A
	1304 (+111)	A
	1348 (+155)	A
HXeI···HBr	1281.0 (+87.8)	C
	1302.7 (+109.5)	A
	1349.9 (+156.7)	A
HXeI···HI	1230.4 (+37.2)	B
	1268.0 (+74.8)	A
	1289.2 (+96.0)	A
HXeI···H_2C_2	1242 (+49)	A
	1248 (+55)	A

[a] Monomer-to-complex frequency shifts (in cm^{-1}) are shown in parenthesis. The data for the HXeI···HI and HXeI···HBr complexes are from Ref. 71.

The HXeI monomer and the HXeI···HCl and HXeI···HCCH complexes can be decomposed by IR radiation of the spectrometer (Figure 12). The lifetime of these species under the IR irradiation was obtained by fitting the decay curves by a single exponent. Figure 13 shows the lifetimes of the HXeI monomer and the HXeI complexes with HI ,[71] HBr,[71] HCl, and HCCH as a function of the monomer-to-complex shift of the H–Xe stretching mode. It is seen that the photostability of these species increases with the H–Xe stretching frequency.

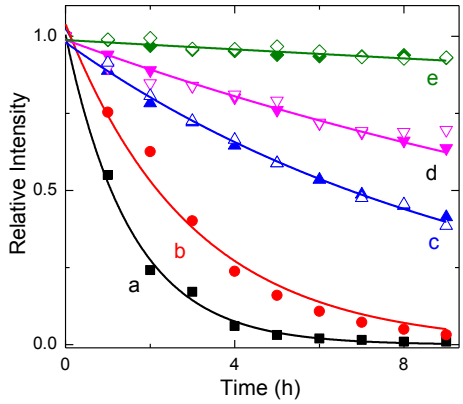


Figure 12. *Time dependences of the normalized absorption intensities of the HXeI, HXeI···HCCH, and HXeI···HCl species under broadband IR radiation: (a) HXeI monomer (ν_{H-Xe} at 1193 cm^{-1}); (b) HXeI···HCCH complex (ν_{H-Xe} at 1242 cm^{-1}); (c) HXeI···HCl complex (ν_{H-Xe} at 1287 cm^{-1} and ν_{H-Cl} at 2651 cm^{-1}); (d) HXeI···HCl complex (ν_{H-Xe} at 1304 cm^{-1} and ν_{H-Cl} at 2586 cm^{-1}); (e) HXeI···HCl complex (ν_{H-Xe} at 1348 cm^{-1} and ν_{H-Cl} at 2501 cm^{-1}). The lines are single exponential fits of the H–Xe stretching intensities. In plots c–e, the solid symbols stand for HXeI and the open symbols for HCl.*

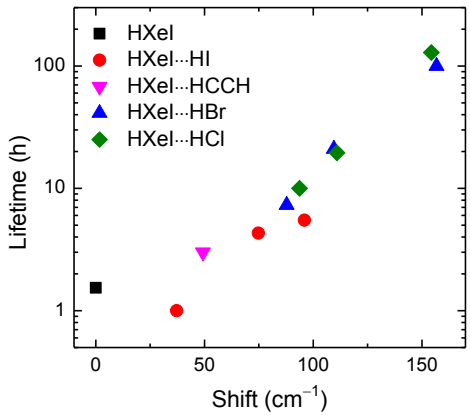


Figure 13. *Lifetime of HXeI in different complexes under broadband IR radiation of the spectrometer as a function of the monomer-to-complex shift of the H−Xe stretching mode. The data for the HXeI···HI and HXeI···HBr complexes are from Ref. 71.*

4.1.3 Discussion

The synthesis of the HNgY···M complexes (M is an interacting molecule) in a matrix includes photolysis of the HY···M precursors to produce the H + Y···M fragments and subsequent

annealing to promote the H + Ng + Y···M → HNgY···M reaction.[66] In this thesis, the HXeI···HCl and HXeI···HCCH complexes have been studied. The HI···HCl and HCl···HI complexes are the precursors of the HXeI···HCl complex and the HCCH···HI complex is the precursor of the HXeI···HCCH complex. The intensities of the bands assigned to the HXeI···HCl and HXeI···HCCH complexes correlate with the amounts of their precursors observed after matrix deposition.

For the HXeI···HCl complex in a Xe matrix, the H–Xe stretching bands are shifted by +94, +111, and +155 cm^{-1} from the HXeI monomer (Table 9) and the HCl stretching bands are shifted by –187, –252, and –337 cm^{-1} from the *Q* branch of the HCl monomer. The relative intensities of these bands are independent of the HCl concentration; thus, they all belong to the 1:1 complex. No indications of the HXeCl···HI complex are found, which is probably because of the less efficient photodecomposition of HCl as compared with HI.

All bands observed for HXeI···HCl are assigned to the energetically most stable structure A based on the comparison of the experimental and calculated spectra (Tables 8 and 9). The experimental shifts of the H–Xe and HCl stretching modes (up to +155 and –337 cm^{-1}) agree better with the calculated values for structure A (+166.7 and –265.6 cm^{-1}, CCSD(T)) than for structure B (Tables 8 and 9). Furthermore, the intensity ratio of the H–Xe and HCl stretching modes calculated for structure A (2.0) also agrees with the experimental value (2.5). Structural perturbations caused by different matrix morphologies (matrix-site effect) are probably the reason for the large splitting of the HCl and H–Xe stretching bands. An extensive band splitting has also been reported for the HKrCl···HCl,[68] HXeI···HI, and HXeI···HBr complexes.[71] The detailed explanation of this matrix-site effect is a challenge for computational chemistry.

For HXeI···HCCH, the H–Xe stretching band is shifted by +49 cm^{-1} from the HXeI monomer. This band is assigned to structure A because the CCSD(T) method predict only this structure for this complex. The calculated shift (+103.5 cm^{-1} at the CCSD(T) level and +70.1 cm^{-1} at the MP2(full) level) reasonably agrees with the experiment. The observed small discrepancy may be due to the matrix effect and/or the computational error. The non-observation of the bands of complexed HCCH can be explained by the much lower intensities of its vibrations compared to the intensity of the H–Xe stretching mode of HXeI (Table 8).

For structure A, the interaction energies (without ZPVE correction, at the CCSD(T) level of theory) of the HXeI···HCl (–4.94 kcal mol^{-1}) and HXeI···HBr (–4.69 kcal mol^{-1}) complexes are similar. On the other hand, these interaction energies are substantially greater than those of the HXeI···HI (–3.88 kcal mol^{-1}) and HXeI···HCCH (–3.10 kcal mol^{-1}) complexes. In accord, the H–Xe stretching shifts of the HXeI···HCl (up to +155 cm^{-1}) and HXeI···HBr (up to +154 cm^{-1}) complexes are also similar and substantially larger than those of the HXeI···HI (up to +96 cm^{-1}) and HXeI···HCCH (+49 cm^{-1}) complexes. These results indicate that the interaction

energy of the complexes correlates with the complexation effect (in this case, with the H–Xe stretching frequency).

The photostability of the HXeI complexes is another interesting issue. The lifetime of HXeI in different complexes under broadband IR radiation of the spectrometer strongly increases with the H−Xe stretching frequency (Figure 13). Two mechanisms can be responsible for this effect. The first mechanism is connected to an increase of the harmonicity of the H–Xe stretching mode upon complexation. Pettersson *et al*. have proposed that the decomposition of HXeI occurs via absorption at the second H–Xe stretching overtone in the 2950–3800 cm^{-1} region.[149] The intensity of this overtone of the HXeI complexes presumably decreases as the H–Xe stretching frequency increases, which in turn decreases the decomposition rate. Indeed, the calculations show that the intensity of the *first* overtone of the HXeI···HCCH and HXeI···HCl complexes is about 55 and 30% of that of the HXeI monomer.[III] The differences between the intensities of the *second* overtone are probably larger; however, these values cannot be calculated by the used program. The second proposed mechanism originates from the different excess energies available for the H atom after photodissociation. Our estimates show that the excess energy for the H atom is about 500 cm^{-1} smaller for the HXeI···HCl complex than for the HXeI monomer.[III] This change presumably decreases the cage exit probability of the H atom for the complex and hence increases the probability of the back-reaction.

4.2 Matrix effect on HXeI and HXeH

4.2.1 Computational results

The calculations are performed for the HXeY monomer and HXeY···Ng complexes in vacuum and for HXeY (Y = H and I) in noble-gas (Ar, Kr, and Xe) lattices. The results in noble-gas matrices are obtained using the hybrid quantum-classical simulations.[92,150]

The H–Xe bond lengths and H–Xe stretching frequencies of HXeI and HXeH are given in Table 10. The harmonic H–Xe stretching frequency of HXeI (1354 cm^{-1}) is in good agreement

Table 10. *H–Xe bond lengths (in Å) and H–Xe stretching harmonic and anharmonic frequencies (in cm^{-1}) of HXeI and HXeH in vacuum.*[a]

	Bond length	Harmonic frequency	Anharmonic frequency
HXeI	1.769	1354	1131
HXeH	1.941	1211 (asymmetric)	1138 (asymmetric)

[a]The equilibrium bond lengths and anharmonic frequencies are calculated using the discrete variable representation (DVR) method. The harmonic frequencies of HXeI and HXeH are calculated using the CCSD(T) and CASPT2 methods, respectively.

with the CCSD(T) calculations by Tsuge *et al.* (1327 cm^{-1}).[71] The anharmonic calculation decreases the H–Xe stretching frequency of HXeI by ~200 cm^{-1} (to 1131 cm^{-1}). For the HXeH monomer, the treatment of anharmonic vibrational motion decreases the asymmetric H–Xe stretching frequency by ~80 cm^{-1} (to 1138 cm^{-1}).

For the HXeY···Ng complexes, the calculations are performed with fixed internal coordinates of HXeY.[IV] Three minima have been located for the HXeI···Ng complex: two collinear (H-side and I-side) and bent structures. For the HXeH···Ng complex, the collinear and bent structures are also obtained.

For HXeY in matrix environments, the calculated stabilization energy and anharmonic H–Xe stretching frequencies in the <110> and <100> sites are presented in Table 11. For HXeI, the <110> site is lower in energy in all matrices. For HXeH, the <110> site is slightly lower in energy in an Ar matrix and higher in energy in Kr and Xe matrices compared to the <100> site. In all cases, the obtained H–Xe stretching frequencies in the matrices are blue-shifted from the values in vacuum.

Figure 14 shows the contour plots of the two-dimensional distribution functions of noble-gas atoms around HXeI in the <110> site and HXeH in the <100> sites. The molecular axis of HXeY is taken as the *x* axis and *r* is the distance from the *x* axis. The positions of noble-gas atoms in the HXeY···Ng complexes (collinear and bent structures) are also shown.

Table 11. *Calculated anharmonic H–Xe stretching frequencies (in cm^{-1}) and stabilization energies (ΔE, in kcal mol^{-1}) of HXeI and HXeH in Ar, Kr, and Xe matrices.*[a]

	<110>				<100>			
	N_r	Freq.	Shift	Δ*E*	N_r	Freq.	Shift	Δ*E*
HXeI								
Ar matrix	2	1357	+226	−8.9	2	1278	+147	−5.1
Kr matrix	2	1361	+230	−11.2	2	1277	+146	−4.4
Xe matrix	2	1327	+196	−11.1	1	1414	+283	−3.2
HXeH								
Ar matrix	2	1151	+13	−3.6	1	1190	+52	−3.2
Kr matrix	2	1162	+24	−3.4	1	1177	+39	−4.5
Xe matrix	2	1152	+14	−2.7	1	1154	+16	−5.9

[a] N_r is the number of noble-gas atoms substituted with HXeI or HXeH. The frequency shifts from the values obtained in vacuum (HXeI: 1131 cm^{-1}, HXeH: 1138 cm^{-1}) are also shown.

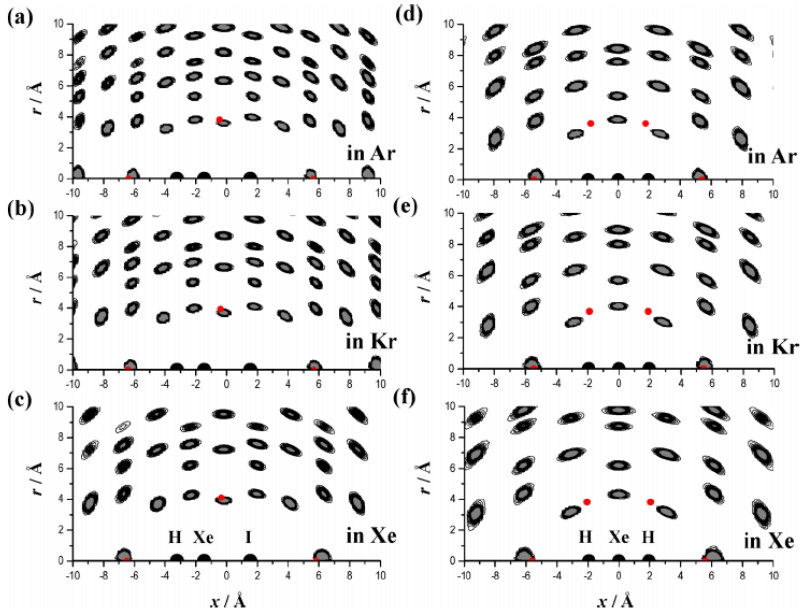


Figure 14. *Contour plots of two-dimensional distribution functions of the Ng atoms around (a-c) HXeI in the <110> site and (d-f) HXeH in the <100> site in Ar, Kr, and Xe matrices. The positions of HXeI and HXeH in the minimum energy structures in vacuum are represented by black circles. The positions of the noble-gas atoms in the isolated HXeI···Ng and HXeH···Ng complexes are shown by red circles.*

4.2.2 Experimental results

HI monomer absorbs at 2253.5 and 2245.0 cm^{-1} in an Ar matrix and at 2239.5 and 2233 cm^{-1} in a Kr matrix.[151] Addition of Xe leads to the formation of the HI···Xe complex absorbing at 2233.1 cm^{-1} in a Ar matrix and at 2222.0 cm^{-1} in a Kr matrix. The HI monomer absorption in a Xe matrix consists of several bands separated by 2–3 cm^{-1}.[146] About 600 pulses of 193-nm light decompose practically all HI molecules.

Subsequent annealing of the photolyzed matrix at ~20 K (in an Ar matrix) and at ~30 K (in an Kr matrix) mobilizes H atoms and leads to the formation of HXeI and HXeH in these matrices (Figure 15). To recall, annealing at 40 K of a photolyzed HI/Xe matrix produces HXeI and HXeH in a Xe matrix. The attempts to prepare these molecules in a Ne matrix were unsuccessful. The H–Xe stretching frequencies of HXeI and HXeH in different matrices are given in Table 12.

Several experiments have been performed to confirm these assignments. For example, the bands of HXeI and HXeH in Ar and Kr matrices are efficiently decomposed by UV light at 193 nm and by a mercury lamp (254 nm), which is characteristic of noble-gas hydrides.[25] Without adding Xe, these bands are absent in the photolyzed and annealed Ar and Kr matrices.

Irradiation at 488 nm bleaches only the bands of HXeI in Ar, Kr, and Xe matrices whereas the bands of HXeH are quite insensitive to this radiation (Figure 11). In HBr/Xe/Ar and HBr/Xe/Kr matrices, in addition to HXeBr (1541 and 1524 cm^{-1} in Ar and Kr matrices, respectively),[22,90] the bands assigned in this work to HXeH also appear after photolysis and annealing and they are easily decomposed by UV light.

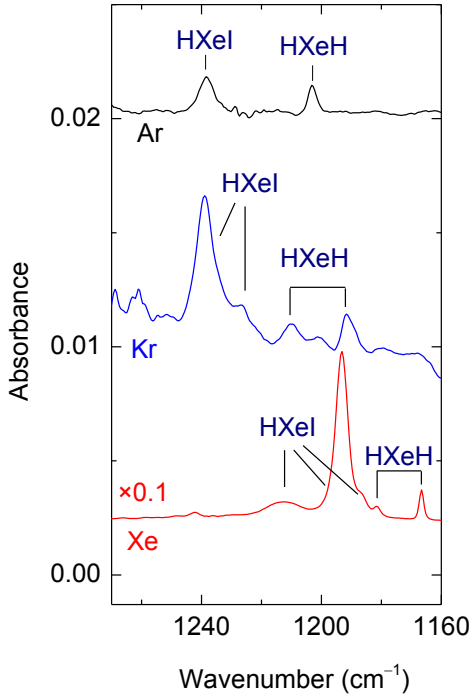


Figure 15. *HXeI and HXeH in different matrices. FTIR difference spectra show the results of annealing of photolyzed HI/Xe/Ar, HI/Xe/Kr, and HI/Xe matrices at 20, 30, and 40 K, respectively. The spectra are measured at 3 K.*

Table 12. *Experimental H–Xe stretching frequencies (in cm^{-1}) of HXeI and HXeH in Ar, Kr, and Xe matrices.*[a]

	Ar	Kr	Xe
HXeI	1238.0 (+45.0)	1239.0 (+46.0) 1227.3(weak)	1193.0 1213 (weak), 1186.7 (weak)
HXeH	1203.2(+37.3)	1192.1 (+26.2) 1209.9 (weaker)	1165.9 1181.5 (weaker)

[a]The shift in parenthesis is calculated with respect to the strongest bands of HXeI and HXeH in a Xe matrix.

4.2.3 Discussion

The synthesis of HXeI in Ar and Kr matrices includes photolysis of the HI···Xe complex to produce the H + I···Xe fragments and subsequent annealing to promote the H + Xe···I → HXeI reaction. HXeH molecules also appear in these experiments. The annealing-induced formation of HXeH probably consists of two steps: H + Xe → Xe···H and H + Xe···H → HXeH.

The observed H–Xe stretching bands of HXeI are at 1238.0 in an Ar matrix and at 1239.0 cm^{-1} in a Kr matrix, which are blue-shifted from the band in a Xe matrix (1193.0 cm^{-1}) by 45.0 and 46.0 cm^{-1}. These shifts are larger than the corresponding values for HXeCl (27 and 16 cm^{-1})[22,91] and for HXeBr (37 and 23 cm^{-1}).[22,90] This trend shows that the matrix effect is stronger for less stable HNgY molecules. It is seen that the order of H–Xe stretching frequencies of HXeI is ν(Xe) < ν(Ar) < ν(Kr), which is qualitatively different from that found previously for HXeCl, HXeBr, and HXeCCH (ν(Xe) < ν(Kr) < ν(Ar)).[22,89-91]

The observed H–Xe stretching bands of HXeH at 1203.2 and 1192.1 cm^{-1} in Ar and Kr matrices (the strongest band is given for a Kr matrix) are blue-shifted from the strongest band of HXeH in a Xe matrix (1166 cm^{-1}) by 37.3 and 26.2 cm^{-1}. Tsuge *et al.* reported that the H–Xe stretching band of HXeH in a N_2 is only slightly shifted (by +10.7 cm^{-1}) from the strongest band at 1166 cm^{-1} in a Xe matrix.[90] This weak environmental effect on HXeH was connected with its symmetric structure. However, our results show that the frequency changes for HXeH in different noble-gas matrices are comparable to those for HXeI. The order of the H–Xe stretching frequencies of HXeH in the various matrices is different from that of HXeI but the same as of HXeCl, HXeBr, and HXeCCH.[22,89-91] The second (weaker) band of HXeH in a Kr matrix at 1210 cm^{-1} is also observed. The interval between the two bands of HXeH in a Kr matrix (18 cm^{-1}) is similar to that in a Xe matrix (15 cm^{-1}). This splitting is probably induced by the matrix-site effect and the two matrix configurations seem to be similar in Kr and Xe matrices. Only one matrix site for HXeH appears in an Ar matrix.

The calculations of the 1:1 HXeY···Ng complexes (Y = I and H, Ng = Ar, Kr, and Xe) fail to explain the experimental results in different matrices,[IV] similarly to the cases of HXeBr and HXeCCH.[89,90] Thus, larger systems should be considered to simulate the matrix effect. The hybrid quantum-classical simulations for HXeI and HXeH in noble-gas lattices successfully describe the main experimental results. For HXeI, the <110> site is preferred because it is reliably lower in energy than the <100> site. The calculated shifts of the H–Xe stretching mode in Ar and Kr matrices from that in a Xe matrix (+30 and +34 cm^{-1}) agree well with the experimental results (+45 and +46 cm^{-1}). The calculated H–Xe stretching frequency order for HXeI in these matrices agrees with the experiment (ν(Xe) < ν(Ar) < ν(Kr)). On the other hand, the calculations overestimate the absolute values of the H–Xe stretching frequency by ~130 cm^{-1} (Tables 11 and 12).

For HXeH, the <110> (double substitution) site is slightly lower in energy only in an Ar matrix whereas the <100> (single substitution) site is reliably lower in energy in Kr and Xe matrices. If we use the lower energy sites in all matrices, the order of the calculated H–Xe stretching frequencies disagrees with the experiments results (ν(Xe) < ν(Kr) < ν(Ar) while considering the stronger bands in Kr and Xe matrices). On the other hand, the simulation for the <100> site successfully reproduce the experimental results. The calculated frequency shifts obtained in Ar and Kr matrices with respect to a Xe matrix (+36 and +23 cm^{-1}) are in excellent agreement with the experiments (+37.3 and +26.2 cm^{-1}). The present calculations cannot explain the appearance of two bands of HXeH in Kr and Xe matrices. The calculated frequencies are in good absolute agreement with the experiment (error 10–15 cm^{-1}).

The H–Xe stretching frequency in Ar and Kr matrices are blue-shifted with respect to that in a Xe matrix for both HXeI and HXeH. This trend can be explained by the computational results. We compare the distances between the "external" noble-gas atom and the H atom of HXeY in the matrix environments and in the H-side 1:1 complexes. Figure 14 shows that this distance is smaller in Ar and Kr matrices relative to the 1:1 complexes whereas it is relatively larger for a Xe matrix. The H–Xe stretching frequency is strongly affected by noble-gas atoms beside the H atom of HNgY in the collinear geometry.[IV] When the noble-gas atom is located closer to the H atom, the repulsion between the noble-gas atom and the embedded molecule increases, which subsequently increases the H–Xe stretching frequency. Kalinowski *et al.*[91] has also suggested that the different sizes of the noble-gas cages are responsible for the observed matrix effects on the H–Xe stretching frequency. From this point of view, the size of the embedded molecule can also affect the frequency shifts. This may explain why the H–Xe stretching frequency order of HXeI is different from other noble-gas hydrides studied previously (HXeCl, HXeBr, and HXeCCH).[22,87-91]

The failure to prepare HXeI and HXeH in a Ne matrix is worth commenting. The calculations show that the stabilization energies of HXeI are negative in Ar, Kr, and Xe matrices but it is positive in a Ne matrix.[IV] This positive stabilization energy may be a reason for the absence of HXeI in a Ne matrix. Other possibilities for this failure include the intrinsic instability of HXeI and HXeH and/or relatively high formation barriers.

5. Results in brief

This thesis consists of two parts: (i) investigation of new noble-gas compounds and (ii) study of the environmental effects on selected noble-gas hydrides.

In the first part, we identify new noble-gas compounds in solid matrices using IR spectroscopy. The compounds under study belong to two types: HNgY and YNgY' where Ng is a noble-gas atom and Y and Y' are electronegative fragments. The experimental assignments are supported by *ab initio* calculations at the MP2(full) and CCSD(T) levels of theory with the def2-TZVPPD basis set.

We have prepared and characterized two new HNgY compounds (noble-gas hydrides): HKrCCCl in a Kr matrix and HXeCCCl in a Xe matrix.[I] The synthesis of these compounds includes two steps: UV photolysis of HCCCl in a noble-gas matrix to form the H + CCCl fragments and annealing of the matrix to mobilize H atoms and to promote the H + Ng + CCCl $\rightarrow$ HNgCCCl reaction. An interesting observation in the experiments on HXeCCCl in a Xe matrix is the temperature-induced transformation of the three H–Xe stretching bands. This observation is explained by temperature-induced changes of local matrix morphology around the embedded HXeCCCl molecule. In these experiments, we have also obtained the IR spectrum of the CCCl radical, which is produced by photodecomposition of HCCCl.

We have identified three new YNgY' compounds (fluorinated noble-gas cyanides): FKrCN in a Kr matrix and FXeCN and FXeNC in a Xe matrix.[II] These molecule are formed by photolysis of FCN in a noble-gas matrix due to locality of this process. The amount of these molecules increases upon thermal mobilization of the F atoms in the photolyzed matrix featuring the F + Ng + CN reaction.

The precursors used to prepare these noble-gas compounds (HCCCl or FCN) are produced by a microwave discharge of a mixture of $HClC{=}CCl_2$ or $(FCN)_3$ with the noble gas. This method allows one to deposit matrices containing highly reactive species that are otherwise difficult to synthesize.

In the second part of this thesis, we investigate the environmental effects on noble-gas compounds. More specifically, the complexation effect on HXeI and the matrix effect on HXeI and HXeH are studied.

Two new complexes HXeI···HCl and HXeI···HCCH have been prepared in a Xe matrix and assigned based on the *ab initio* calculations at the MP2(full) and CCSD(T) levels of theory.[III] The HXeI complexes are produced by UV photolysis of HI/HY/Xe (Y = Cl or CCH) matrices to form the H + I···HY fragments and annealing of the matrix to promote the H + Xe + I···HY $\rightarrow$ HXeI···HY reaction. The H–Xe stretching mode in the complexes is blue-shifted with respect to the HXeI monomer by 49 cm^{-1} (HXeI···HCCH) and up to 155 cm^{-1} (HXeI···HCl).

The decomposition of the HXeI complexes by broadband IR radiation of the spectrometer is found to be slower than that of the HXeI monomer. Moreover, the decomposition rate of the HXeI complexes systematically decreases as the H–Xe stretching frequency increases. The same trend occurs for the previously studied HXeI···HBr and HXeI···HI complexes.[71] Two mechanisms are proposed to explain the observed effect.

HXeI and HXeH in Ar, Kr, and Xe matrices have been prepared.[IV] The order of the H–Xe stretching frequency of HXeH (ν(Xe) < ν(Kr) < ν(Ar)) is the same as that of HXeCl, HXeBr, and HXeCCH studied previously.[22,89-91] For HXeI, the frequency order is somewhat different, ν(Xe) < ν(Ar) < ν(Kr), which is a remarkable observation. The hybrid quantum-classical calculations successfully simulate these experimental results.

References

[1]W. Kossel, Ann. Phys. **49**, 229 (1916).

[2]A. von Antropoff, Z. Angew. Chem. **37**, 217 (1924).

[3]L. Pauling, J. Am. Chem. Soc. **55**, 1895 (1933).

[4]N. Bartlett, Proc. Chem. Soc. 218 (1962).

[5]C. L. Chernick, H. H. Claassen, J. G. Malm, and P. L. Plurien, *Noble-Gas Compounds*, University of Chicago Press, Chicago (1963).

[6]H. Selig, J. G. Malm, and H. H. Claassen, Sci. Am. **210**, 66 (1964).

[7]J. G. Malm, H. Selig, J. Jortner, and S. A. Rice, Chem. Rev. **65**, 199 (1965).

[8]J. G. Malm and E. H. Appelman, At. Energy Rev. **7**, 3 (1969).

[9]V. K. Brel, N. S. Pirguliyev, and N. S. Zefirov, Usp. Khim. **70**, 262 (2001).

[10]W. Grochala, Chem. Soc. Rev. **36**, 1632 (2007).

[11]W. Grochala, L. Khriachtchev, and M. Räsänen, in *Physics and Chemistry at Low Temperatures*, edited by L. Khriachtchev (Pan Stanford Publishing, Singapore, 2011), Chap. 13, pp. 419–446.

[12]J. Haner and G. J. Schrobilgen, Chem. Rev. **115**, 1255 (2015).

[13]L. Y. Nelson and G. C. Pimentel, Inorg. Chem. **6**, 1758 (1967).

[14]C. T. Goetsche and K. R. Loos, J. Am. Chem. Soc. **94**, 3018 (1972).

[15]R. D. Leblond and D. D. Desmarteau, J. Chem. Soc., Chem. Commun. 555 (1974).

[16]L. J. Turbini, R. E. Aikman, and R. J. Lagow, J. Am. Chem. Soc. **101**, 5833 (1979).

[17]S. Seidel and K. Seppelt, Science **290**, 117 (2000).

[18]J. F. Lehmann, H. P. A. Mercier, and G. J. Schrobilgen, Coord. Chem. Rev. **233**, 1 (2002).

[19]J. J. Turner, and G. C. Pimentel, Science **140**, 974 (1963).

[20]G. J. Schrobilgen, J. Chem. Soc., Chem. Commun. 863 (1988).

[21]J. C. P. Sanders and G. J. Schrobilgen, J. Chem. Soc., Chem. Commun. 1576 (1989).

[22]M. Pettersson, J. Lundell, and M. Räsänen, J. Chem. Phys. **102**, 6423 (1995).

[23]M. Pettersson, J. Lundell, and M. Räsänen, J. Chem. Phys. **103**, 205 (1995).

[24]L. Khriachtchev, M. Pettersson, N. Runeberg, J. Lundell, and M. Räsänen, Nature **406**, 874 (2000).

[25]L. Khriachtchev, M. Räsänen, and R. B. Gerber, Acc. Chem. Res. **42**, 183 (2009).

[26]R. Baumfalk, N. H. Nahler, and U. Buck, J. Chem. Phys. **114**, 4755 (2001).

[27]N. H. Nahler, M. Farnik, and U. Buck, Chem. Phys. **301**, 173 (2004).

[28]V. Poterya, O. Votava, M. Farnik, M. Oncak, P. Slavicek, U. Buck, and B. Friedrich, J. Chem. Phys. **128**, 104313 (2008).

[29]V. I. Feldman, F. F. Sukhov, A. Y. Orlov, and I. V. Tyulpina, J. Am. Chem. Soc. **125**, 4698 (2003).

[30]V. I. Feldman, F. F. Sukhov, A. Y. Orlov, I. V. Tyul'pina, E. A. Logacheva, and D. A. Tyurin, Russ. Chem. B **54**, 1458 (2005).

[31]V. I. Feldman, A. V. Kobzarenko, A. Y. Orlov, and F. F. Sukhov, Low Temp. Phys. **38**, 766 (2012).

[32]S. V. Ryazantsev, A. V. Kobzarenko, and V. I. Feldman, J. Chem. Phys. **139**, 124315 (2013).

[33]S. V. Kameneva, A. V. Kobzarenko, and V. I. Feldman, Radiat. Phys. Chem. **110**, 17 (2015).

[34]A. Lignell, L. Khriachtchev, J. Lundell, H. Tanskanen, and M. Räsänen, J. Chem. Phys. **125**, 184514 (2006).

[35]L. Khriachtchev, A. Domanskaya, J. Lundell, A. Akimov, M. Räsänen, and E. Misochko, J. Phys. Chem. A **114**, 4181 (2010).

[36]W. F. Howard, Jr. and L. Andrews, J. Am. Chem. Soc. **96**, 7864 (1974).

[37]T. Arppe, L. Khriachtchev, A. Lignell, A. V. Domanskaya, and M. Räsänen, Inorg. Chem. **51**, 4398 (2012).

[38]G. Q. Liu, L. Wang, X. X. Zhang, and W. X. Zhang, Comput.Theor. Chem. **974**, 31 (2011).

[39]J. L. Chen, C. Y. Yang, H. J. Lin, and W. P. Hu, Phys. Chem. Chem. Phys. **15**, 9701 (2013).

[40]S. Borocci, M. Giordani, and F. Grandinetti, J. Phys. Chem. A **118**, 3326 (2014).

[41]L. L. Ma, Z. G. Huang, X. Q. Niu, B. H. Zhang, and Q. Wang, Inorg. Chim. Acta. **414**, 210 (2014).

[42]S. Pan, A. Gupta, S. Mandal, D. Moreno, G. Merino, and P. K. Chattaraj, Phys. Chem. Chem. Phys. **17**, 972 (2015).

[43]G. C. Pimentel and A. L. McClellan, Annu. Rev. Phys. Chem. **22**, 347 (1971).

[44]K. Muller-Dethlefs and P. Hobza, Chem. Rev. **100**, 143 (2000).

[45]E. R. Johnson, S. Keinan, P. Mori-Sanchez, J. Contreras-Garcia, A. J. Cohen, and W. T. Yang, J. Am. Chem. Soc. **132**, 6498 (2010).

[46]P. Hobza and K. Müller-Dethlefs, *Non-Covalent Interactions: Theory and Experiment*, The Royal Society of Chemistry, Cambridge, England (2010).

[47]B. S. Ault and G. C. Pimentel, J. Phys. Chem. **77**, 1649 (1973).

[48]A. J. Barnes, J. B. Davies, H. E. Hallam, and J. D. R. Howells, J. Chem. Soc., Faraday Trans. 2 **69**, 246 (1973).

[49]A. J. Barnes, J. Mol. Struct. **60**, 343 (1980).

[50]B. Nelander, J. Chem. Phys. **72**, 77 (1980).

[51]M. W. Hnat, Z. Mielke, Z. Latajka, and H. Ratajczak, Spectrochim. Acta, Part A **38**, 1259 (1982).

[52]A. J. Barnes, J. Mol. Struct. **100**, 259 (1983).

[53]A. Engdahl and B. Nelander, Chem. Phys. Lett. **100**, 129 (1983).

[54]Z. Mielke, J. Phys. Chem. **88**, 3288 (1984).

[55]V. E. Bondybey, and J. H. English, J. Mol. Spectrosc. **109**, 221 (1985).

[56]H. B. Bai and B. S. Ault, J. Phys. Chem. **98**, 10001 (1994).

[57]Z. Mielke, K. G. Tokhadze, Z. Latajka, and E. Ratajczak, J. Phys. Chem. **100**, 539 (1996).

[58]A. Engdahl and B. Nelander, Chem. Phys. **249**, 215 1999).

[59]A. Heikkilä, M. Pettersson, J. Lundell, L. Khriachtchev, and M. Räsänen, J. Phys. Chem. A **103**, 2945 (1999).

[60]N. A. Young, Coord. Chem. Rev. **257**, 956 (2013).

[61]L. Khriachtchev, J. Phys. Chem. A **119**, 2735 (2015).

[62]A. V. Nemukhin, B. L. Grigorenko, L. Khriachtchev, H. Tanskanen, M. Pettersson, and M. Räsänen, J. Am. Chem. Soc. **124**, 10706 (2002).

[63]A. Lignell, L. Khriachtchev, M. Pettersson, and M. Räsänen, J. Chem. Phys. **117**, 961 (2002).

[64]A. Lignell, L. Khriachtchev, M. Pettersson, and M. Räsänen, J. Chem. Phys. **118**, 11120 (2003).

[65]H. Tanskanen, S. Johansson, A. Lignell, L. Khriachtchev, and M. Räsänen, J. Chem. Phys. **127**, 154313 (2007).

[66]A. Lignell and L. Khriachtchev, J. Mol. Struct. **889**, 1 (2008).

[67]A. Lignell, J. Lundell, L. Khriachtchev, and M. Räsänen, J. Phys. Chem. A **112**, 5486 (2008).

[68]A. Corani, A. Domanskaya, L. Khriachtchev, M. Räsänen, and A. Lignell, J. Phys. Chem. A **113**, 10687 (2009).

[69]L. Khriachtchev, S. Tapio, M. Räsänen, A. Domanskaya, and A. Lignell, J. Chem. Phys. **133**, 084309 (2010).

[70]M. Tsuge, S. Berski, R. Stachowski, M. Räsänen, Z. Latajka, and L. Khriachtchev, J. Phys. Chem. A **116**, 4510 (2012).

[71]M. Tsuge, S. Berski, M. Räsänen, Z. Latajka, and L. Khriachtchev, J. Chem. Phys. **138**, 104314 (2013).

[72]M. Tsuge, S. Berski, M. Räsänen, Z. Latajka, and L. Khriachtchev, J. Chem. Phys. **140**, 044323 (2014).

[73]K. Willmann, T. Vent-Schmidt, M. Räsänen, S. Riedel, and L. Khriachtchev, RSC Adv. **5**, 35783 (2015).

[74]S. A. C. McDowell, Phys. Chem. Chem. Phys. **5**, 808 (2003).

[75]S. A. C. McDowell, Chem. Phys. Lett. **377**, 143 (2003).

[76]J. Lundell, S. Berski, and Z. Latajka, Chem. Phys. Lett. **371**, 295 (2003).

[77]R. B. Gerber, Annu. Rev. Phys. Chem. **55**, 55 (2004).

[78]S. A. C. McDowell, Curr. Org. Chem. **10**, 791 (2006).

[79]L. Sheng and R. B. Gerber, J. Chem. Phys. **126**, 021108 (2007).

[80]S. A. C. McDowell and G. S. Volney, J. Chem. Phys. **136**, 124306 (2012).

[81]C. Cheng and L. Sheng, Comput. Theor. Chem. **989**, 39 (2012).

[82]R. B. Gerber, E. Tsivion, L. Khriachtchev, and M. Räsänen, Chem. Phys. Lett. **545**, 1 (2012).

[83]E. Tsivion and R. B. Gerber, Phys. Chem. Chem. Phys. **13**, 19601 (2011).

[84]A. J. Barnes, H. E. Hallam, and G. F. Scrimsha, Trans. Faraday Soc. **65**, 3159 (1969).

[85]A. J. Barnes and J. D. R. Howells, J. Chem. Soc., Faraday Trans. 2 **68**, 729 (1972).

[86]A. J. Barnes and Z. Mielke, J. Mol. Struct. **1023**, 216 (2012).

[87]M. Lorenz, M. Räsänen, and V. E. Bondybey, J. Phys. Chem. A **104**, 3770 (2000).

[88]L. Khriachtchev, H. Tanskanen, J. Lundell, M. Pettersson, H. Kiljunen, and M. Räsänen, J. Am. Chem. Soc. **125**, 4696 (2003).

[89]H. Tanskanen, L. Khriachtchev, J. Lundell, and M. Räsänen, J. Chem. Phys. **125**, 074501 (2006).

[90]M. Tsuge, A. Lignell, M. Räsänen, and L. Khriachtchev, J. Chem. Phys. **139**, 204303 (2013).

[91]J. Kalinowski, R. B. Gerber, M. Räsänen, A. Lignell, and L. Khriachtchev, J. Chem. Phys. **140**, 094303 (2014).

[92]K. Niimi, A. Nakayama, Y. Ono, and T. Taketsugu, J. Phys. Chem. A **118**, 380 (2014).

[93]K. Niimi, T. Taketsugu, and A. Nakayama, Phys. Chem. Chem. Phys. **17**, 7872 (2015).

[94]L. Khriachtchev, H. Tanskanen, A. Cohen, R. B. Gerber, J. Lundell, M. Pettersson, H. Kiljunen, and M. Räsänen, J. Am. Chem. Soc. **125**, 6876 (2003).

[95]M. Pettersson, J. Nieminen, L. Khriachtchev, and M. Räsänen, J. Chem. Phys. **107**, 8423 (1997).

[96]E. Whittle, D. A. Dows, and G. C. Pimentel, J. Chem. Phys. **22**, 1943 (1954).

[97]I. Norman and G. Porter, Nature **174**, 508 (1954).

[98]H. E. Hallam, *Vibrational Spectroscopy of Trapped Species: Infrared and Raman Studies of Matrix-Isolated Molecules, Radicals and Ions*, John Wiley & Sons, New York (1973).

[99]L. Andrews and M. Moskovits, *Chemistry and Physics of Matrix-Isolated Species*, North-Holland, Amsterdam (1989).

[100]A. Utsunomiya, K. Sasaki, Y. Tanaka, M. Omura, and N. Tomoshige, U.S. patent 5,693,306 (2 December 1997).

[101]F. Jensen, *Introduction to Computational Chemistry*, John Wiley & Sons, Chichester, England (1999).

[102]C. Møller and M. S. Plesset, Phys. Rev. **46**, 618 (1934).

[103]B. H. Besler, G. E. Scuseria, A. C. Scheiner, and H. F. Schaefer, J. Chem. Phys. **89**, 360 (1988).

[104]D. Rappoport and F. Furche, J. Chem. Phys. **133**, 134105 (2010).

[105]D. Feller, J. Comput. Chem. **17**, 1571 (1996).

[106]K. A. Peterson, D. Figgen, E. Goll, H. Stoll, and M. Dolg, J. Chem. Phys. **119**, 11113 (2003).

[107]H.-J. Werner, P. J. Knowles, F. R. Manby, and M. Schütz, *et al.*, MOLPRO, version 2010.1, a package of *ab initio* programs, 2010, see http://www.molpro.net.

[108] F. Weinhold, in *Encyclopedia of Computational Chemistry,* edited by P. v. R. Schleyer, N. L. Allinger, T. Clark, J. Gasteiger, P. A. Kollman, H. F. Schaefer III, and P. R. Schreiner (Wiley, Chichester, UK, 1998), Vol. 3, pp. 1792−1811.

[109]M. J. Frisch, G. W. Trucks, and H. B. Schlegel, *et al.*, GAUSSIAN 09, Revision B.01, Gaussian, Inc., Wallingford, CT, 2009.

[110]I. G. Kaplan, *Intermolecular Interactions: Physical Picture, Computational Methods and Model Potentials*, John Wiley & Sons, Chichester, England (2006).

[111]S. F. Boys and F. Bernardi, Mol. Phys. **19**, 553 (1970).

[112]J. Echave and D. C. Clary, Chem. Phys. Lett. **190**, 225 (1992).

[113]H. Tanskanen, L. Khriachtchev, J. Lundell, H. Kiljunen, and M. Räsänen, J. Am. Chem. Soc. **125**, 16361 (2003).

[114]A. Engdahl and B. Nelander, J. Mol. Struct. **193**, 101 (1989).

[115]S. Hirabayashi and K. M. T. Yamada, J. Chem. Phys. **122**, 244501 (2005).

[116]H. Tanskanen, L. Khriachtchev, J. Lundell, and M. Räsänen, J. Chem. Phys. **121**, 8291 (2004).

[117]I. Mincu, M. Hillebrand, A. Allouche, M. Cossu, P. Verlaque, J. P. Aycard, and J. Pourcin, J. Phys. Chem. **100**, 16045 (1996).

[118]L. Khriachtchev, M. Pettersson, and M. Räsänen, Chem. Phys. Lett. **288**, 727 (1998).

[119]V. E. Bondybey and G. C. Pimentel, J. Chem. Phys. **56**, 3832 (1972).

[120]H. M. Kunttu and J. A. Seetula, Chem. Phys. **189**, 273 (1994).

[121]J. Szczepanski, S. Ekern, C. Chapo, and M. Vala, Chem. Phys. **211**, 359 (1996).

[122]K. I. Dismuke, W. R. M. Graham, and W. Weltner, J. Mol. Spectrosc. **57**, 127 (1975).

[123]H. Kunttu, J. Seetula, M. Räsänen, and V. A. Apkarian, J. Chem. Phys. **96**, 5630 (1992).

[124]M. E. Jacox and D. E. Milligan, J. Chem. Phys. **43**, 866 (1965).

[125]G. Maier and C. Lautz, Eur. J. Org. Chem. **1998**, 769 (1998).

[126]D. Forney, M. E. Jacox, and W. E. Thompson, J. Mol. Spectrosc. **170**, 178 (1995).

[127]L. Khriachtchev, M. Saarelainen, M. Pettersson, and M. Räsänen, J. Chem. Phys. **118**, 6403 (2003).

[128]J. Eberlein and M. Creuzburg, J. Chem. Phys. **106**, 2188 (1997).

[129]L. Khriachtchev, H. Tanskanen, M. Pettersson, M. Räsänen, V. Feldman, F. Sukhov, A. Orlov, and A. F. Shestakov, J. Chem. Phys. **116**, 5708 (2002).

[130]L. Khriachtchev, M. Pettersson, J. Lundell, H. Tanskanen, T. Kiviniemi, N. Runeberg, and M. Räsänen, J. Am. Chem. Soc. **125**, 1454 (2003).

[131]T. Shimanouchi, J. Phys. Chem. Ref. Data **6**, 993 (1977).

[132]A. D. Abbate and C. B. Moore, J. Chem. Phys. **82**, 1255 (1985).

[133]J. Lundell and M. Räsänen, J. Phys. Chem. **99**, 14301 (1995).

[134]F. Stroh, B. Winnewisser, M. Winnewisser, H. Reisenauer, G. Maier, S. Goede, and F. Bickelhaupt, Chem. Phys. Lett. **160**, 105 (1989).

[135]D. E. Milligan and M. E. Jacox, J. Chem. Phys. **47**, 278 (1967).

[136]G. Schallmoser, A. Thoma, B. Wurfel, and V. Bondybey, Chem. Phys. Lett. **219**, 101 (1994).

[137]M. Pettersson, J. Lundell, L. Khriachtchev, and M. Räsänen, J. Chem. Phys. **109**, 618 (1998).

[138]J. Lundell, L. Khriachtchev, M. Pettersson, and M. Räsänen, Low Temp. Phys. **26**, 680 (2000).

[139]L. Khriachtchev, M. Pettersson, A. Lignell, and M. Räsänen, J. Am. Chem. Soc. **123**, 8610 (2001).

[140]M. Pettersson, L. Khriachtchev, A. Lignell, M. Räsänen, Z. Bihary, and R. B. Gerber, J. Chem. Phys. **116**, 2508 (2002).

[141]A. V. Bochenkova, V. E. Bochenkov, and L. Khriachtchev, J. Phys. Chem. A **113**, 7654 (2009).

[142]M. Pettersson, L. Khriachtchev, J. Lundell, S. Jolkkonen, and M. Räsänen, J. Phys. Chem. A **104**, 3579 (2000).

[143]L. Khriachtchev, M. Pettersson, J. Lundell, and M. Räsänen, J. Chem. Phys. **114**, 7727 (2001).

[144]R. Tarroni and S. Carter, J. Chem. Phys. **123**, 014320 (2005).

[145]R. Tarroni, L. Khriachtchev, A. Domanskaya, M. Räsänen, E. Misochko, and A. Akimov, Chem. Phys. Lett. **493**, 220 (2010).

[146]M. Pettersson, L. Khriachtchev, R. J. Roozeman, and M. Räsänen, Chem. Phys. Lett. **323**, 506 (2000).

[147]M. Räsänen, J. Seetula, and H. Kunttu, J. Chem. Phys. **98**, 3914 (1993).

[148]H. Tanskanen, L. Khriachtchev, M. Räsänen, V. I. Feldman, F. F. Sukhov, A. Y. Orlov, and D. A. Tyurin, J. Chem. Phys. **123**, 064318 (2005).

[149]M. Pettersson, J. Nieminen, L. Khriachtchev, and M. Räsänen, J. Chem. Phys. **107**, 8423 (1997).

[150]A. Nakayama, K. Niimi, Y. Ono, and T. Taketsugu, J. Chem. Phys. **136**, 054506 (2012).

[151]M. T. Bowers and W. H. Flygare, J. Chem. Phys. **44**, 1389 (1966).